



**ISLAMIC UNIVERSITY OF TECHNOLOGY**  
**ORGANISATION OF ISLAMIC COOPERATION**



# **NANOFLUID IMPLEMENTATION IN HEAT EXCHANGER GEOMETRIES**

SUBMITTED IN PARTIAL FULFILLMENT OF THE  
REQUIREMENTS  
FOR THE DEGREE OF  
**BACHELOR OF SCIENCE IN MECHANICAL ENGINEERING**

**AUTHORED BY,**

**Foyez Ahmad**

Student ID: 170011060

**Sajjad Mahmud**

Student ID: 170011064

Supervised By,

**Dr. Mohammad Monjurul Ehsan**


**DEPARTMENT OF MECHANICAL AND PRODUCTION  
ENGINEERING**

MAY- 2022

# CERTIFICATE OF RESEARCH

*This thesis titled "NANOFLUID IMPLEMENTATION IN HEAT EXCHANGER GEOMETRIES" submitted by FOYEZ AHMAD (170011060) and SAJJAD MAHMUD (170011064) has been accepted as satisfactory in partial fulfillment of the requirement for the Degree of Bachelor of Science in Mechanical Engineering.*

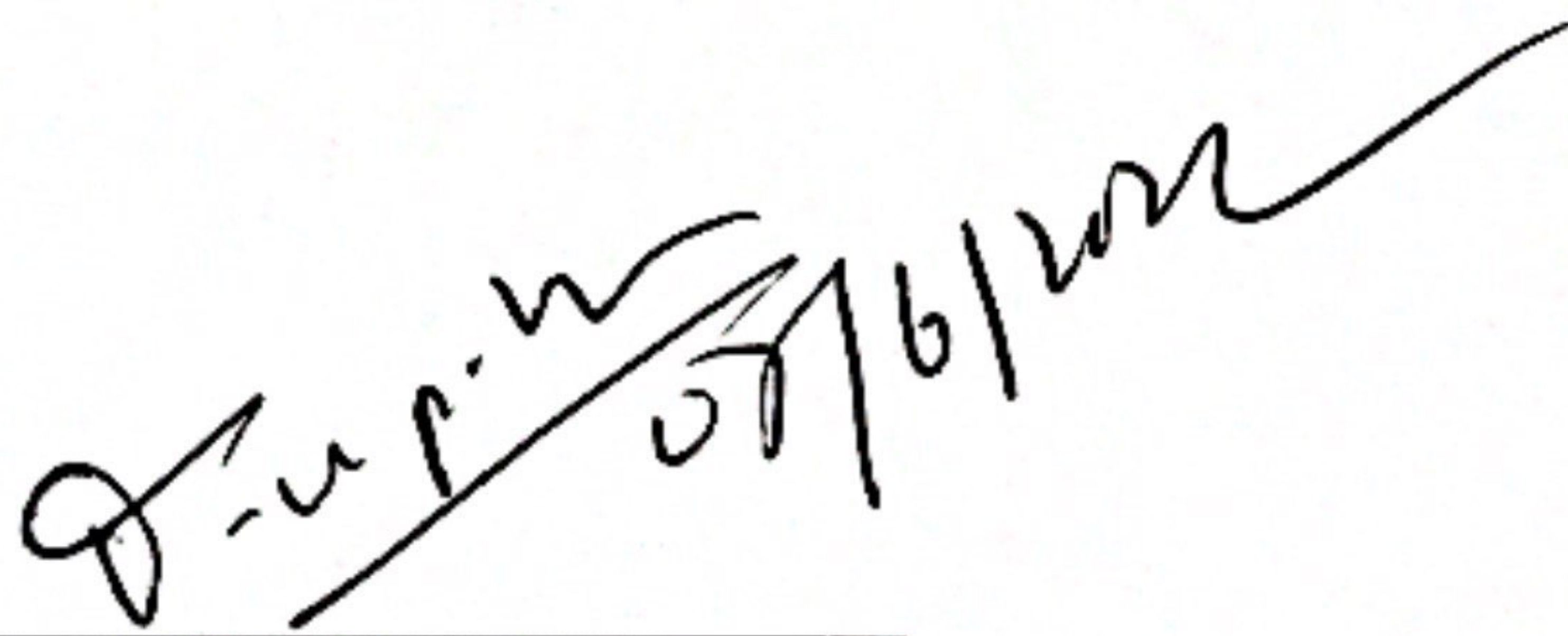
***Supervisor***

  
07.06.2022

**Dr. Mohammad Monjurul Ehsan**

*Associate Professor*

***Head of the Department***

  
07/6/2022

**Dr. Md. Anayet Ullah Patwari**

*Professor*

Department of Mechanical and Production Engineering (MPE)

Islamic University of Technology (IUT)

## DECLARATION

*I hereby declare that this thesis entitled "Nanofluid Implementation in Heat Exchanger Geometries" is an authentic report of study carried out as requirement for the award of degree B.Sc. (Mechanical Engineering) at Islamic University of Technology, Gazipur, Dhaka, under the supervision of Dr. Mohammad Monjurul Ehsan, Associate Professor, MPE, IUT in the year 2022*

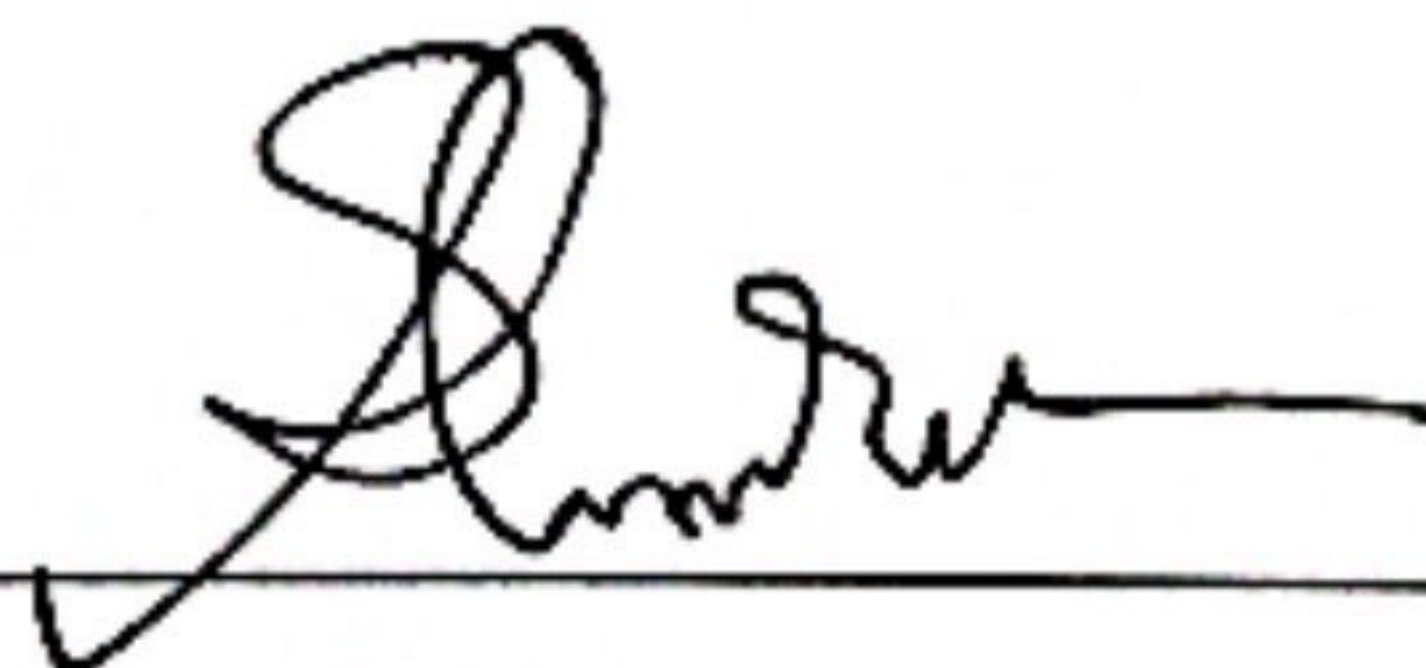
*The matter embodied in this thesis has not been submitted in part or full to any other institute for award of any degree.*



---

**Foyez Ahmad**

**Student ID:170011060**



---

**Sajjad Mahmud**

**Student ID: 170011064**

## **ACKNOWLEDGEMENTS**

First of all, we would like to express earliest gratitude to the almighty Allah (SWT) for his blessings, which allowed them to successfully accomplish this thesis.

We are sincerely grateful to their supervisor Dr. Mohammad Monjurul Ehsan sir, for his continuous guidance, helpful suggestions and supervision throughout this research period and undergraduate study. Whenever we faced difficulties or faced unpredictable problems, he was there with his strong and patient support during the project with his precious advice. His motivation and guidance greatly aided us at every stage of this research study.

And finally, we are appreciative to our family members for their unwavering encouragement and support during their endeavor of a Bachelor of Science in Mechanical Engineering at Islamic University of Technology (IUT).

## Abstract

In recent years, nanotechnology has evolved as an important field that employs sophisticated "green" nanoparticles incorporated in conventional engineering resources. The heat transfer performance of nanofluids is superior to that of traditional heat transfer fluids. Suspending nanoparticles in nanofluids increases the ratio of contact surface to volume. Consequently, they can be placed evenly to maximize heat transfer without incurring a significant decrease in pressure. In the cooling and heating sectors, nanofluids are a preferred heat transfer fluid due to these benefits. The considerable increase in heat conductivity that nanoparticles provide has made nanofluids highly desirable for a variety of energy applications. In the past decade, thermal effects of nanofluids in both forced and free convection flows have been of great interest to researchers. In our current study, we investigated the influence of nanofluid coolants in spherical dimpled surfaces on heat transfer and pressure drop. The primary purpose of this research is to assess the thermal performance of nanofluids with regard to varying Reynolds numbers and nanoparticle volume concentrations in a dimpled channel flow. Assuming a constant and uniform heat flux of  $10000 \text{ w/m}^2$ , the simulations are performed at Reynolds numbers from 10000 to 30000. The computational fluid dynamics solver ANSYS Fluent is used to analyze the effective properties of nanofluids based on models presented in the literature. There is a discussion on the results of heat transfer coefficient, temperature distributions, Nusselt number, pressure drop, and friction factors for all the scenarios. Different nanoparticle compositions were shown to have a 20-25% higher heat transfer coefficient for dimpled channels compared to smooth ones. With increasing volume fractions, it was found that heat transfer and pressure drop values did go up. Nusselt number grows as more complex corrugations are being used. Because the performance evaluation factor (PEF) for corrugated geometries is greater than unity, they can surpass smooth pipes. In addition to the decrease in PEF values, both Re and PEF advances show a decreasing trend as well.

**Keyword:** heat transfer, 3D corrugated pipe, dimpled surface, friction factor, hybrid nanofluid, PEC, heat exchanger

# Table of Contents

<b>ABSTRACT</b> .....	<b>5</b>
<b>NOMENCLATURE</b> .....	<b>11</b>
<b>CHAPTER 1</b> .....	<b>13</b>
<b>INTRODUCTION</b> .....	<b>13</b>
1.1 PROBLEM STATEMENT:.....	13
1.2 STATE OF THE ART: .....	13
1.3 NANOFUID APPLICATIONS .....	15
1.4 PROCEDURE .....	15
<b>CHAPTER 2</b> .....	<b>17</b>
<b>LITERATURE REVIEW</b> .....	<b>17</b>
2.1 REVIEW ON HEAT EXCHANGER:.....	17
2.2 REVIEW ON NANOFUIDS .....	20
<b>CHAPTER 3</b> .....	<b>23</b>
<b>RESEARCH DESIGN</b> .....	<b>23</b>
3.1 CFD MODEL AND SIMULATION.....	23
3.2 PROCEDURE OF NUMERICAL SIMULATION .....	23
3.3 MATHEMATICAL MODELING .....	24
3.4 TURBULENCE MODELLING .....	25
3.5 CONVERGENCE CRITERION .....	26
<b>CHAPTER 4</b> .....	<b>27</b>
<b>DATA GENERATION, ANALYSIS AND DISCUSSION</b> .....	<b>27</b>
4.1 DIMPLED CORRUGATED PIPE .....	27
4.1.1 <i>Description of Computational Domain</i> .....	27
4.1.2 <i>Mesh Configuration</i> .....	28
4.1.3 <i>Grid Sensitivity Analysis</i> .....	30
4.1.4 <i>Physical Flow Parameters and Boundary Condition</i> .....	33
4.1.5 <i>Code Validation</i> .....	33
4.1.6 <i>Thermo-Physical Properties of Nanofluids, Water and Nanoparticles</i> 34	

4.1.7	<i>Data Reduction</i>	38
4.1.8	<i>Flow Behavior Investigations</i>	40
4.1.8.1	Pressure Distribution	40
4.1.8.2	Variation in Flow Velocity	42
4.1.8.3	Temperature Contour	43
4.1.9	<i>Effect of Geometry</i>	43
4.1.9.1	Heat Transfer Performance Analysis	43
4.1.10	<i>Pressure Drop</i>	45
4.1.11	<i>Shear Stress</i>	46
4.1.12	<i>Entropy Generation</i>	47
4.1.13	<i>Performance Evaluation Criterion</i>	49
4.2	<b>DIFFERENT CORRUGATED CHANNELS</b>	51
4.2.1	<i>Description of Computational Domain</i>	51
4.2.1.1	Trapezoidal Fluid Domain	51
4.2.1.2	Sine Shaped Corrugated Fluid Domain	51
4.2.1.3	V-corrugated Fluid Domain	52
4.2.2	<i>Physical Flow Parameters and Boundary Condition</i>	54
4.2.3	<i>Code Validation</i>	54
4.2.4	<i>Flow Behavior Investigations</i>	55
4.2.4.1	Pressure distribution	55
4.2.4.2	Variation in flow velocity	56
4.2.4.3	Temperature contours	57
4.2.5	<i>Effect of Geometry</i>	58
4.2.5.1	Heat Transfer Performance Analysis	58
4.2.5.2	Pressure Drop	60
4.2.5.3	Performance Evaluation Criterion (PEC)	60
	<b>CHAPTER 5</b>	<b>62</b>
	<b>CONCLUSION AND RECOMMENDATION</b>	<b>62</b>
5.1	FINDINGS	62
5.2	LIMITATIONS	63
5.3	FUTURE RECOMMENDATION	64
	<b>REFERENCES</b>	<b>66</b>

## Table of Figures

Figure 1: Convergence criterion of the solver .....	26
Figure 2: Schematic diagram of doubled dimpled corrugated pipe.....	28
Figure 3: Mesh configuration at the tube's cross section and along its length.....	29
Figure 4: Section plane along the radial direction of the corrugated dimple pipe.....	30
Figure 5: Impact of grid refinement on dimpled pipe.....	31
Figure 6: Variation of velocity with varying element size for dimpled pipe at Re = 15000.....	32
Figure 7: Variation of pressure drop with varying element size for dimpled pipe at Re = 15000 .....	32
Figure 8: Physical representation of the solution domain.....	33
Figure 9: validation of numerical and experimental data in a pipe.....	34
Figure 10: Pressure distribution in a corrugated test section from several positions...	40
Figure 11: Swirl flow at the corrugated dimpled section.....	41
Figure 12: Variation in flow velocity in smooth and dimpled pipes (a) smooth pipe, (b) aspect ratio of dimpled configurations 2, (c) aspect ratio 2.5, (d) aspect ratio 3 .....	42
Figure 13: Temperature variations in dimpled corrugated pipe.....	43
Figure 14: Variation of Nusselt number with Reynolds number for different geometries .....	44
Figure 15: Variation of convective heat transfer coefficient with Re for different geometries .....	45
Figure 16: Pressure drop of 1% Al <sub>2</sub> O <sub>3</sub> /H <sub>2</sub> O nanofluid in different geometries.....	45
Figure 17: Wall shear stress of Al <sub>2</sub> O <sub>3</sub> /H <sub>2</sub> O nanofluid in corrugated pipe of AR 2 at Re= 20000.....	46
Figure 18: Variation in volumetric entropy generation for Al <sub>2</sub> O <sub>3</sub> /water .....	47
Figure 19: Variation in volumetric entropy generation for different corrugation configurations for 1% Al <sub>2</sub> O <sub>3</sub> /water.....	48
Figure 20: Variations in Nu/Nu <sub>0</sub> and with Reynolds Number .....	50
Figure 21: Variations in PEC with Reynolds Number.....	50
Figure 22: Geometry of the trapezoidal fluid domain .....	51



Figure 23: Geometry of the sine shaped fluid domain.....	51
Figure 24: Geometry of the V-shaped fluid domainMesh Configuration.....	52
Figure 25:Mesh configuration at different corrugated channel's cross section and along its length (a) sine shaped, (b) trapezoidal, (c) V-shapedGrid Sensitivity Analysis.....	53
Figure 26:Variation of Nusselt Number with varying element size for trapezoidal channel at $Re = 15000$ .....	53
Figure 27:The solution domain as a representation of its physical state .....	54
Figure 28: validation of numerical data in a corrugated channel.....	55
Figure 29:Pressure drop across (a) trapezoid, (b) sine-shaped, (c) V-shaped corrugated section .....	56
Figure 30:Variation in flow velocity in (a) trapezoid, (b) sine-shaped and (c) V- shaped corrugated channel.....	57
Figure 31:Temperature contours in trapezoidal corrugated channel .....	58
Figure 32: Variation of Nusselt number with Reynolds number for different geometries .....	59
Figure 33:Variation of convective heat transfer coefficient with $Re$ for different geometries .....	59
Figure 34:Pressure drop in different geometries.....	60
Figure 35:The effects of different values of the trapezoidal-corrugated channel's amplitude to wavelength ratio on $PEC$ .....	61

## List of Tables

Table 1: Properties of water and nanoparticles .....	36
Table 2: Thermophysical properties of Al <sub>2</sub> O <sub>3</sub> /water .....	37
Table 3: Thermophysical properties of CuO/water .....	38
Table 4: Thermophysical properties of Al <sub>2</sub> O <sub>3</sub> -CuO/water.....	38
Table 5: Thermophysical properties of Al <sub>2</sub> O <sub>3</sub> -TiO <sub>2</sub> /water .....	38
Table 6: PEC of Al <sub>2</sub> O <sub>3</sub> -H <sub>2</sub> O nanofluid in different configurations .....	49

## Nomenclature

$A_c$	Cross sectional area
$A_s$	Surface area
$C_p$	Specific heat
$D_h$	Hydraulic diameter
$Re$	Reynolds number
$Pr$	Prandtl number
$Nu$	Nusselt number
$h$	Heat transfer coefficient
$k$	Thermal conductivity
$T_{in}$	Inlet temperature
$T_{out}$	Outlet temperature
$T_{mean}$	Mean Temperature
$T_{wall}$	Wall temperature
$V_{in}$	Inlet velocity
HTC	Heat transfer coefficient
PEC	Performance evaluation criterion
AR	Aspect ratio

### Greek Symbols

$\phi$	Nanoparticle volume fraction
$\mu$	Dynamic viscosity
$\nu$	Kinematic viscosity
$\beta$	Thermal Expansion Coefficient
$\rho$	Density

## Subscript

i, j, k	Tensor index
bf	Base fluid
nf	Nanofluid
w	Wall
h <sub>nf</sub>	Hybrid nanofluid
b	Bulk
np	Nanoparticle
B	Brownian
VWD	Van der waals
avg	Averaged

# CHAPTER 1

## INTRODUCTION

### 1.1 Problem statement:

Heat transfer is one of the most fundamental industrial operations. Heat should be efficiently managed in any industrial facility by transferring to the relevant sectors. Due to their poor thermal performance, traditional heat transfer fluids such as water, ethylene glycol, pumping oil, and others have not demonstrated significant capability for cooling purpose. It has already been shown that adding solid particles to these traditional fluids can improve their thermal performance. However, micrometer or larger particle suspensions are not an effective selection for hightech applications such as micro electronics, data centers, and micro-channels. To solve the inadequacies of conventional fluids, the cooling industry's primary concern is to yield efficient heat transfer fluids. [1] [2]

The cooling technology bottleneck greatly impedes the rapid progress of electronic component downsizing. This necessitates a desperate action, neglecting the evaluation of economic variables in order to improve overall performance. Different scientists took different ways to enhance the performance of heat exchangers. The following elements influence the thermal and hydraulic performance of a HX: diameter, length, obstacle in fluid flow, and coolant. There are several varieties of HX on the market: shell and tube HX, double tube HX, plate HX, compact and so on are examples. The factors connected with material qualities for steady heat transfer also limit the substrate material.

### 1.2 State of The Art:

Such limitations led to an extensive research on cooling medium of heat exchanger. In the last decade, nanoscience and nanotechnology (NFs) have provided new solutions by imparting nanofluids (NFs), which may help to improve the performance of heat transfer fluids, particularly in high-tech applications.

In a heat exchanger, the fluids could be separated by a solid wall to avoid mixing, or they might be in direct or indirect contact. When a furnace is used to burn natural gas or propane fuel, the combustion byproducts (flue gas) enter the heat exchanger and

travel through it. When hot flue gas departs the furnace, the metal is heated up. As this happens, the air is heated by the hot metal that circulates around the outside of the heat exchanger. When designing a component, a heat exchanger is used in almost every industrial application. For example, it is employed in the refrigeration and air conditioning industries, as well as in power plants and even in spacecraft. Heat exchangers come in a wide variety of shapes and sizes and each one was used for a specific case or application. Helical heat exchangers or coil-type heat exchangers are used from the beginning. The helical heat exchanger experiences centrifugal force as a result of its shape. Because of the curvature, which generates secondary flow to aid in fluid mixing, it has a better heat transfer performance than straight pipes.

Heat exchanger equipments are utilized in many industrial settings, such as thermal applications, nuclear power generation, chemical reactors, and numerous other engineering applications, all necessarily involve thermal performance enhancements and modifications in order to minimize their size, cost, and energy consumption [3]–[6]. Corrugated tubes are commonly used in heat exchangers, which are used to transfer heat between fluids of different temperatures [7]–[9]. Heat transfer enhancement can be done by two techniques: passive and active. Active methods necessitate the use of a power supply from outside, surface vibration, and mechanical devices whereas passive methods do not. Passive heat transfer techniques use different types of surface geometries such as rough surfaces, extended surfaces, corrugated surface, as well as displacement enhancement devices or fluid additives to improve heat exchanger performance in a variety of applications [10], [11]. To enhance heat transfer in the pipes, numerous computational and experimental investigations have been accomplished.

NPs (nanometer-sized particles) dispersed in ordinary base fluids form nanofluids, a novel type of solid/liquid mixture. Following to the literature, NPs can be metallic/intermetallic compounds (such as Ag, Cu, Ni and so on) [12]–[16], as well as ceramic compounds such as oxides, sulfides, and carbides. Some nanoshaped ceramic substrate reported in the literature include  $\text{Al}_2\text{O}_3$ ,  $\text{MoS}_2$ ,  $\text{Fe}_2\text{O}_3$ ,  $\text{Fe}_3\text{O}_4$ ,  $\text{CuO}$ ,  $\text{TiO}_2$ ,  $\text{SiO}_2$ ,  $\text{CeO}_2$ ,  $\text{ZnO}$ , mesoporous  $\text{SiO}_2$ ,  $\text{SiC}$ . [17]–[23] Carbon based compounds like carbon nanotubes, graphite, graphene, graphene oxide, and others, can also be nanostructured materials. [24], [25] Water, ethylene glycol (EG), diethylene glycol (DEG), polyethylene glycol, a mixture of water and EG, vegetable and coconut oil,

gear oil, kerosene, paraffin, pump oil, and other base liquids are used. [26]–[30] As shown, this new dispersion is a suspension with three phases: solid phase, solid and liquid interface, and liquid phases. As the introduction of the NF concept more than a decade ago, the opportunities for NFs applications in various areas have gained much attention. As a result, many researches are ongoing in this area for various purposes and applications.

### **1.3 Nanofluid Applications**

One of the most pressing scientific issues in many industries is heat transfer. As a result, among all NF applications, their scope for heat transfer applications has garnered the most attention. [31]. NFs may be used in transportation systems like automobile radiators [32], [33]. They can be used in metal cutting in metal processing [34], [35]. They could also be used to cool data centers and electronics [36].

When it comes to energy saving, several research suggest that NFs can be used as a medium to manufacture advanced phase change materials (PCMs) for thermal energy storage [37] or to absorb sunlight, where NFs could enhance the absorption property of the ordinary working fluid in solar collectors. [37].

The current study introduces new design considerations of HX's geometrical shape by using unique type of corrugation in the geometry and different types of single and hybrid nanofluids are applied. By changing the corrugation dimensions along with aspect ratio of the geometry, and different types of nanofluids along with their change in concentration, heat transfer enhancement were analyzed and compared with the straight pipe. For each geometry, the local Nusselt number has been plotted. Finally, the optimum heat transfer rate with minimum pumping power are calculated among those geometries.

### **1.4 Procedure**

We tried to contribute to this field by introducing different types of hybrid nanofluid on our novel heat exchanger and evaluate its thermal and hydraulic performance compared with water. At first, we validated some works of different nanofluid mixtures

implemented on corrugated heat exchangers. We got a close match with the paper that was used as a reference, and we used this numerical model to go further.

First, the thermal and hydraulic performance of various liquid metal-based Nano fluids is compared to that of water utilizing the same Nano particles at the same particle concentration for our comparative research. Effective cooling performance and overall performance are also evaluated to determine the best base fluid from many aspects. The impact of different nanoparticles is then investigated for various base liquid metal fluids at the same particle concentration. The Nano fluid combination with the greatest heat transfer coefficient is shown in this research. Finally, the influence of particle concentration on thermal and hydraulic performance has been investigated, as well as visual cooling effectiveness inspection and overall performance analysis.



## CHAPTER 2

### LITERATURE REVIEW

#### 2.1 Review on Heat Exchanger:

Cengiz et al. [38] evaluated experimentally the performance of HX by utilizing active and passive mechanisms and investigated the effect of heat transfer on helical corrugated pipes of different configurations for different flow rates; where the dimension of the copper pipes were 10 mm in diameter and 3200 mm in length. The result indicates that greater pressure drop occurred in the effect of rotation of helical tubes.

Corrugation in pipes has been studied by Vicente et al. [39] for its impact on friction factor and heat transfer. Corrugated pipes are a good choice for low Re because they have more pressure drops and enhanced heat transfer than normal smooth pipes; however, tubes with sufficiently more roughness are better for high Re because the friction factor increases up to 300% and the Nu enhances by up to 250%.

Yang et al. [40] and Ma et al. [41] illustrated the effects of corrugated rib with roughened pipe on frictional losses and heat transfer enhancement under various Reynolds numbers ranging from 7500 to 50,000. The results revealed that expanding the gaps with a change in Reynolds number enhanced heat transfer and friction loss. There was an increment in both the Nusselt number and the friction factor to 2.73 and 2.78, correspondingly. [42]

Dong et al. [43] investigated the effect of friction factor along with heat transfer for four different corrugated pipe configurations. The Reynolds numbers used in the investigations varied from 6000 to 93,000 for water and from 3200 to 19,000 for oil. The results revealed that modifying the pipe could raise the heat transfer coefficient and friction factor on the tube side by almost 120% and 160%, correspondingly, when compared to smooth pipes, and thus the corrugated ribs improve heat transfer with the friction factor.

Kwon et al. [44] examined different corrugation angles and their effects on the thermal performance of wavy heat exchangers in two-dimensional flow regimes numerically and experimentally. The performance factor reaches its maximum at an angle of 100

and a Reynolds number of 1000. (1.8). Transient turbulent flow was observed in the channel, which is more frequent as the corrugation angle increases.

To improve heat transfer in corrugated pipes, Zimparov et al.[45] examined the effect of 25 different spiral pitches, measuring anything from 0.44 to 1.18 millimeters in height. Pitch and Reynolds numbers ranged from 6.5 to 16.9 mm and 104 to 624 respectively for the corrugations. The heat transfer increased from 177 percent to 273 percent, while the friction factor jumped from 177 percent to 400 percent.

Vicente et al. [46] examined the thermohydraulic performance of dimpled pipes experimentally with Reynolds numbers ranging from 2000 to 100,000 and Prandtl numbers ranging from 2.5 to 100 in dimpled helical pipes with varying depths and pitches of ten dimple tubes with different geometric dimensions ( $h/d$ ) ranging from 0.08 to 0.12) and ( $p/d$ ) ranging from 0.08 to 0.12). (0.65 to 1.1). Working fluids included water and ethylene glycol. Under the same flow conditions, the smooth pipes experienced a greater pressure drop. The Nusselt number rises by up to 250 percent, while the friction factor coefficient increases by 350 percent. In addition, compression to smooth pipes reduced the surface area by 80%.

Thianpong et al. [47] investigated the thermal performance of 2 dimple tubes with pitch ratios ranging from 0.7 to 1.0 and 3 twisted tapes with twist ratios varying from 3, 5, and 7. They look at how twist ratio ( $y/w$ ) and pitch ratio (PR) affect pressure loss and average heat transfer coefficient [49]. The Reynolds number varied from 12,000 to 44,000. It was discovered that the friction factor and heat transfer coefficient increase as the twist and pitch ratios decrease,. The friction factor and heat transfer coefficient in the enhanced tubes had been found to be higher than in the smooth tube.

Rao et al. [48] investigated the effects of various dimpled shape configurations on thermo-hydraulic performance of the dimpled pin-fin channel both numerically and experimentally. Up to 19 percent of the convective heat transfer performance was enhanced in the case of pin fin-dimple channels, and a higher Nusselt number was found in the wider dimple channel. Furthermore, the friction factors for the improved dimple channels were reduced by up to 17.6 percent.

Bi et al. [49] investigate experimentally the hydrodynamic performance characteristics of a mini-channel heat sink with dimples and cylindrical grooves. The thermal-

hydraulic performance of enhanced tube heat exchangers can be accurately predicted using the appropriate turbulence model.

Xie and Sundén [52] performed numerical simulations of heat transfer augmentation in a rectangular channel with dimples with Reynolds numbers ranging from 100,000 to 600,000. Using the turbulence model, they discovered the greatest heat transfer enhancements. They conclude that the dimpled channel has a 5% additional pressure drop and a 200 percent increase in heat transfer. Their experimental data for dimples with different depth ratios revealed that the augmentation of the heat transfer rate remained nearly constant for different Reynolds numbers.

Lei et al. [50] calculated the impacts of geometrical factors on dimpled tubes such as height and diameter of the dimple, their number, and spacing. The PEC might reach 1.23 at  $Re = 5000$  after a numerical simulation of various dimples with a diameter of 6 mm, a height to diameter ratio of 0.42, and a spacing to diameter ratio of 0.85. The findings indicated that when friction losses rose owing to increases in the surface area of the dimples, which disrupted the flow's velocity boundary layer, the heat transfer rate increased.

To further estimate the connection between thermal-hydraulic performance and pressure loss in dimpled tubes, Fan et al. [51] utilized numerical simulation. The standard  $k$ - $\epsilon$  model was used to predict the turbulent flow. Their findings revealed that decreasing the pitch of the dimples improved heat transfer.

Using a finite volume approach, Esmaeili et al. [52] investigated the flow of  $Al_2O_3$ -water nanofluid in a sinusoidal wavy channel. The results showed that the action of the nanoparticles considerably improved heat transmission. Furthermore, the Nusselt number grew as the Reynolds number increased.

Pandey and Nema [53] investigated the convective heat transfer and flow properties of an  $Al_2O_3$ -water nanofluid in a wavy-plate heat exchanger. It was discovered that raising the Reynolds number and Peclet number improves heat transmission. Furthermore, as the volume percentage of nanoparticles grows, so does the pumping power.

Khoshvaght-Aliabadi et al. [54] investigated the effect of several types of nanofluid on heat transmission performance in a corrugated channel where the test was carried out

at a constant wall temperature and encompassed volume fractions ranging from 0.1 to 0.4 percent. The results revealed that the HTC rose as the volume percentage of nanoparticles increased.

Rosaguti et al. [55] investigated heat transfer and flow dynamics in periodic serpentine channels with semicircular cross-sections where their research was carried out on a wide range of Reynolds number, geometries, and fluid Prandtl numbers. The study's main finding was that the most sophisticated vortical flow patterns occur, and the number and intensity of vortices grow as Re rises.

Tokgoz et al. [56] studied the flow hydrodynamics and heat transfer rate of corrugated channels computationally and experimentally by evaluating two distinct phase shifts. The study used particle image velocimetry to examine the flow structure through the tested channels. The results demonstrated that the formation of vortices in corrugated channels improved heat transport and resulted in lower thermal boundary layers as compared to flat channels.

The heat transmission of alumina nanofluid over a sinusoidal wavy channel was studied by Esmaeili et al. [52]. According to the researchers' results, the nanofluid has a good effect on enhancing the wall's heat transfer enhancement and specific surface area (SS). As a result, the Nu number gets a boost as Re goes up.

According to Ajeel et al. [57]–[59], height to width ratio had a greater influence on PEC than pitch to length ratio. In addition, it is shown that the flow topologies alter when and Re are increased.

## **2.2 Review on Nanofluids**

Narrein and Mohammed [60] investigated four different nanofluids ( $\text{Al}_2\text{O}_3$ ,  $\text{SiO}_2$ ,  $\text{CuO}$ , and  $\text{ZnO}$ ) in a rotating coiled tube heat exchanger with water, ethylene glycol, and engine oil as base fluids. In this study, the Nusselt number was found to be the highest when using  $\text{CuO}$ –water nanofluid.

M.A. Khairul et al. [61] conducted a numerical study on a water-based nanofluid in a helically coiled heat exchanger with no rotation. They concluded that as the volume concentration of nanofluid increases.  $\text{CuO}$ /water nanofluids could increase the heat transfer coefficient by 7.14 percent while decreasing entropy generation by 6.14

percent. By introducing nanoparticles just into the base fluid, it is possible to improve the mass flow rate for the same volume flow rate, resulting in greater efficiency.

Srinivas and Vinod [62] investigated three different water-based nanofluids in a shell and helical heat exchanger. They discovered that larger values of nanofluid concentration, stirrer speed resulted in significant enhancement on heat exchanger effectiveness. Comparing to water, they observed a maximum increase in heat exchanger effectiveness of 30.37 percent, 32.7 percent, and 26.8 percent for  $\text{Al}_2\text{O}_3$ ,  $\text{CuO}$ , and  $\text{TiO}_2$ /water nanofluids, respectively, indicating enhanced heat transfer.

Kannadasan et al. [63] tested  $\text{CuO}$  water-based nanofluids in horizontal and vertical helical heat exchangers with varying volume concentrations. They discovered no significant differences in convective heat transfer coefficients when constructing the horizontal and vertical helical heat exchangers. They also discovered that when the volume concentration is high and the flow rate is low, the friction factor increases.

Shafahi et al. [64] used three different nanofluids,  $\text{Al}_2\text{O}_3$ ,  $\text{CuO}$ , and  $\text{TiO}_2$ , to examine the thermal performance in a two-dimensional heat pipe. They discovered that the nanoparticles in the liquid improve the heat pipe's thermal performance by lowering thermal resistance while increasing the maximum heat. They also discovered that the smaller the nanoparticles, the greater the temperature gradient along the heat pipe.

Wu et al. [65] employed five different percentages of alumina nanofluids to study the pressure drop of a double pipe helical heat exchanger. The heat transfer enhancement of nanofluids over water ranges from 0.37 percent to 3.43 percent based on a fixed flow speed.

Suresh et al. [66] tested the thermophysical properties of a thermochemically synthesized  $\text{Al}_2\text{O}_3$ - $\text{Cu}$ /water hybrid nanofluid in various volume fractions ranging from 0.1 to 2 percent and compared them to theoretical correlation values. Consequently, they showed that in case of hybrid nanofluids, the thermal conductivity is higher than that of mono nanofluids but lower than the calculated values theoretically. They discovered that the  $\text{Al}_2\text{O}_3$ - $\text{Cu}$ /water hybrid nanofluid has a higher viscosity.

Aparna et al. [67] conducted an experimental study on the thermal conductivity of an  $\text{Al}_2\text{O}_3$ - $\text{Ag}$ /water hybrid nanofluid. The volume concentration of nanofluids was increased from 0.005% to 0.10%, and the mixture ratios of  $\text{Al}_2\text{O}_3$ - $\text{Ag}$  nanoparticles

were 50:50, 30:70, and 70:30, respectively. Thermal conductivity increases when volume fraction or temperature increases in nanofluids. The temperature influence on nanofluid thermal conductivity was more evident at increasing particle volume concentrations. It is possible to estimate the thermal conductivity of the tested hybrid nanofluid based on temperature and particle volume fraction, according to the researchers in their study.

Sundar et al. [68] developed a MWCNT-Fe<sub>3</sub>O<sub>4</sub> nanocomposite water-based nanofluid and showed a 29% improvement in thermal conductivity at 0.3 percent volume concentration at 60 °C. In addition, [64] studied and dissolved Al<sub>2</sub>O<sub>3</sub>-Cu nanocomposite powder in Distilled water to obtain a homogenous 0.1 percent volume concentration of the water-based nanofluid. In testing the heat transfer properties of an Al<sub>2</sub>O<sub>3</sub>-Cu nanocomposite nanofluid at a concentration of 0.1 percent volume, the researchers found that the resulting Nusselt number was 13.56 percent higher than that of water when the Reynolds number was the same.

Huang et al. [69] observed an increase in pressure drop characteristics and heat transfer coefficient in plate heat exchangers using a 2.5:1 mixture of Al<sub>2</sub>O<sub>3</sub>-H<sub>2</sub>O and MWCNT-H<sub>2</sub>O nanofluids.

Kumar et al. [70] conducted energy and exergy analysis on plate heat exchangers with different plate spacings using Cu-Al<sub>2</sub>O<sub>3</sub>-H<sub>2</sub>O hybrid nanofluid and found that 5mm spacing provided the best results.

Bhattad et al. [71] investigated a plate heat exchanger with various corrugation with Al<sub>2</sub>O<sub>3</sub>-MWCNT-H<sub>2</sub>O hybrid nanofluid and discovered a 39.16 percent increase in heat transfer coefficient.

Bhattad et al. [72], [73] investigated the energy, exergy, and economics of plate heat exchangers using brine-based hybrid nanofluids for low-temperature applications and discovered that Al<sub>2</sub>O<sub>3</sub>-MWCNT hybrid nanofluid which is based on propylene glycol performs better.

## CHAPTER 3

### RESEARCH DESIGN

#### 3.1 CFD Model and Simulation

CFD is the study of numerically solving engineering problems involving transport phenomena, a subject deals with mathematics. The computational fluid dynamics CFD technique is capable of modeling complicated flow aspects and presenting the results in a visual manner that can be compared to experimental data.

Ansys is a commercial solver program that can also be used to solve CFD issues. Ansys Fluent enhances the capability of computational fluid dynamics analysis. A fluid simulation platform with lightning-fast pre-processing and solution times that enables us to be first to market. The industry-leading capabilities of Ansys Fluent enable limitless creativity without sacrificing accuracy. The ANSYS Fluent software is used in this work to model the intricate flow in a pipe with various geometric forms. Nanoparticles' near-wall behavior is an important consideration in this simulation.

#### 3.2 Procedure of Numerical Simulation

Thermal conductivity and specific heat are considered constant in three dimensional model. With the finite volume technique, the turbulence model and the Navier–Stokes equations can be discretized in the workplace. In the case of tetrahedral and convective terms, the central differencing techniques are employed. Pressure–velocity and solver pressure-based are coupled using SIMPLE's approach. With a second-order upwind discretization method [77][78], all equations related to flow, momentum, and energy are discretized.

In addition, the  $10^{-6}$  value of residual is applied to all calculation variables. In this study, computational models of 3D smooth and corrugated pipes with single-phase turbulent flow are used [79], [80]. Using a numerical solver, the flow equations and heat transfer equations are all solved using water's properties as a working fluid. The turbulent flow in the pipe is studied using a RNG k–turbulent model [81].

The simulations were based on the following assumptions:

1. The flow was in a three-dimensional steady state.
2. The nanofluid is not compressible.
3. The nanoparticles and the base fluid had the same velocity and were in thermal equilibrium.
4. The heat loss to the environment was minimum.
5. The pipes were completely smooth with no roughness
6. Natural convection was insignificant.
7. The thermophysical properties of hybrid nanofluid were stable and independent of temperature.

### 3.3 Mathematical Modeling

As part of ANSYS Fluent's numerical solution of the RANS equations, a Reynolds stress model has been included (RSM). Numerical calculation is utilized to calculate turbulence and heat flow in smooth and various corrugated pipe geometric designs. The pressure profile of the radial stream, comprising the pressure drop, radial, axial, and axial velocities, are calculated in the Reynolds stress model. Both an internal forced vortex and an external free vortex are projected to form in the pipe. [82]

The governing equations' conservation can be stated as follows [83], [84]:

**Continuity equation:**

$$\frac{\partial}{\partial x_i}(u_i) = 0 \quad (1)$$

**Momentum equation:**

$$\frac{\partial(\rho u_i u_j)}{\partial x_i} = -\frac{\partial p}{\partial x_i} + \frac{\partial}{\partial x_j} \left[ \mu \left( \frac{\partial u_i}{\partial x_j} + \frac{\partial u_j}{\partial x_i} - \frac{2}{3} \delta_{ij} \frac{\partial u_i}{\partial x_j} \right) \right] + \frac{\partial}{\partial x_j} (-\rho u_i' u_j') \quad (2)$$

**Energy equation:**

$$\frac{\partial}{\partial x_j} (u_i (\rho E + p)) = \frac{\partial}{\partial x_j} \left[ \left( \lambda + \frac{C_p \mu_t}{Pr_t} \right) - \frac{\partial T}{\partial x_j} + u_i (\tau_{ij})_{eff} \right] \quad (3)$$



$$E = C_p T - \left(\frac{P}{\rho}\right) + \frac{u^2}{2} \quad (4)$$

$$(\tau_{ij})_{eff} = \left[ \mu_{eff} \left( \frac{\partial u_j}{\partial x_i} + \frac{\partial u_i}{\partial x_j} \right) - \frac{2}{3} \mu_{eff} \frac{\partial u_i}{\partial x_j} \delta_{ij} \right] \quad (5)$$

Here,

E = Total energy ;  $(\tau_{ij})_{eff}$  = Stress tensor

The equations for solving the turbulent kinetic energy and the turbulent frequency are listed below. [85]

$$\frac{\partial}{\partial x_i} (k u_i) = -\frac{1}{\rho} \left( \frac{\partial}{\partial x_j} \left( \Gamma_k \frac{\partial k}{\partial x_j} \right) + \widehat{G}_k - Y_k + S_k \right) \quad (6)$$

$$\frac{\partial}{\partial x_j} (\rho \omega u_j) = \frac{1}{\rho} \left( \frac{\partial}{\partial x_j} \left( \Gamma_\omega \frac{\partial \omega}{\partial x_j} \right) + G_\omega - Y_\omega + D_\omega + S_\omega \right) \quad (7)$$

### 3.4 Turbulence Modelling

In general, there is no turbulence model that can be applied to all issues in the field of computational fluid dynamics. In order to find a good turbulence model, multiple sources might be taken into account. Among these are the physics underlying the flow field, the processing time and cost, and the precision. Consequently, it is crucial to comprehend the structure of turbulence models for the utilization in practical applications.

One of the goals of this study is to evaluate the applicability of the various RANS-based turbulence models for forecasting the transient and turbulent characteristics of

nanofluids moving through a pipe-like physical shape. Literature suggests that a Realizable model typically requires somewhat more CPU time than a Standard model when comparing the computing time required by each method for flow modeling. Simulating turbulent flow with a RNG model is significantly more costly and requires around 10-15 percent more CPU time than the Standard model [85].

### 3.5 Convergence Criterion

To check the convergence of the numerical analysis, two distinct types of assessment were conducted. The first was quantitative convergence that was evaluated by observing all residuals. The alternative strategy, known as qualitative convergence, consisted of examining any variable at a specific boundary of the numerical model.[86]

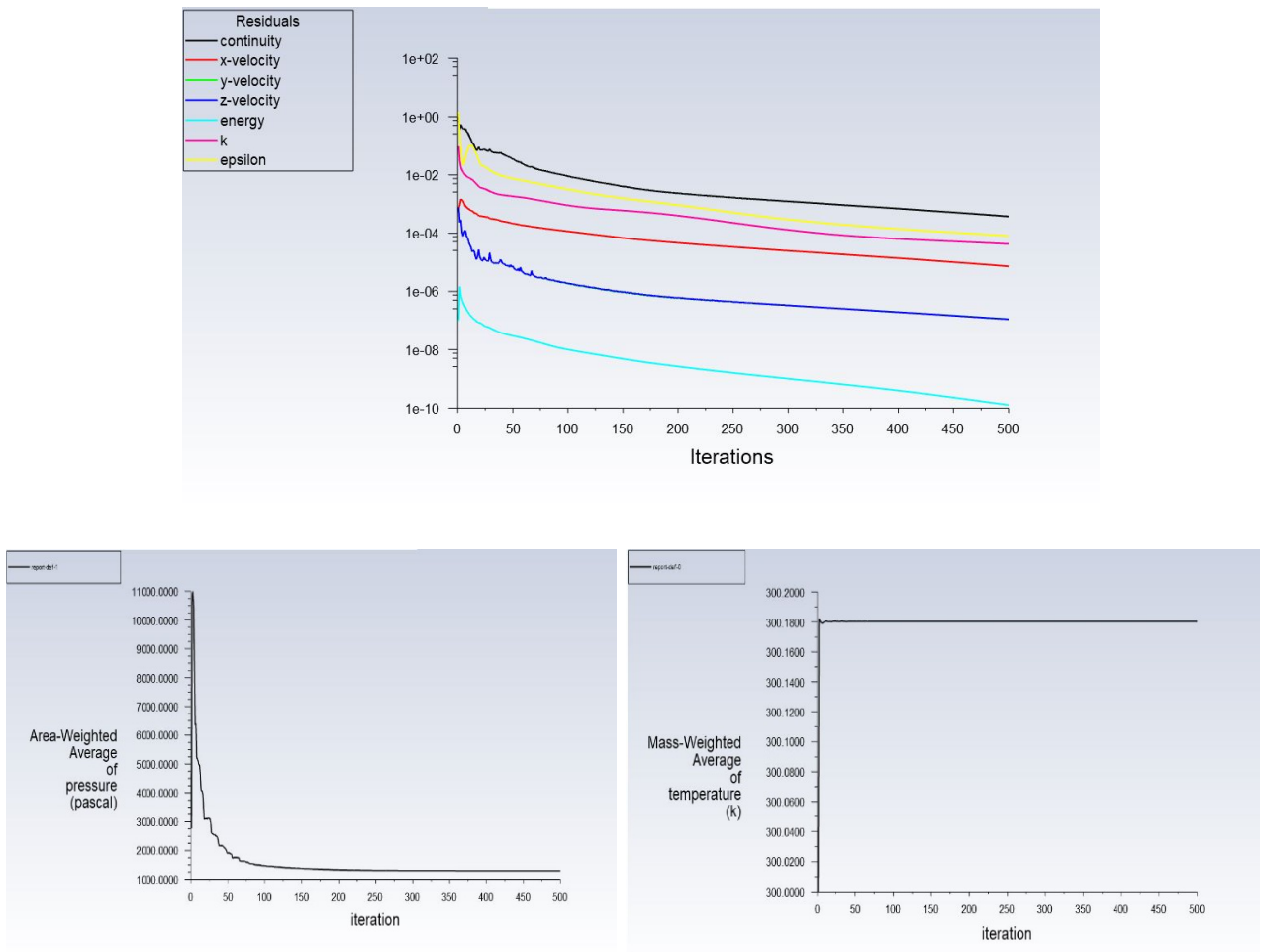


Figure 1: Convergence criterion of the solver

## CHAPTER 4

### DATA GENERATION, ANALYSIS AND DISCUSSION

#### 4.1 Dimpled Corrugated Pipe

##### *4.1.1 Description of Computational Domain*

Passive technologies utilizing various techniques such as dimple and corrugation layouts are becoming increasingly efficient at increasing the efficiency of pipes heat exchangers while lowering expenses. CFD software is utilized to build the computational domain geometry for smooth pipe, dimpled pipe with corrugated surface. A corrugated tube is used to introduce input fluid into the computational domain. The present study presents alternative corrugation patterns on the pipe wall sides in order to alter the intensity of swirl flows and fluid flow. The corrugation flow structure is investigated on the entire pipe wall using a range of Re numbers between 10000 and 30000. In addition, the influence of specific corrugation design combinations on the corrugated pipe will be evaluated. The diameter of the pipe (D) and the length of the flow path (L) are 10 mm and 700 mm, respectively. This investigation employed a three-dimensional view of both smooth and double dimpled pipes, as illustrated in Figure 2. Dimple rows of different diameters, including 0.5, 0.75, and 1.125 mm in various layouts, are uniformly attached to the wall pipe. The length and diameter of each pipe are the same, but the corrugation patterns are different for each pipe. The length of the entry section is 300mm while the corrugated section is 150mm and the exit section is 250mm. The inlet and exit pipes are utilized to increase flow in order to eliminate backflow entirely. The boundary conditions specify the average entry velocity, which is determined based on the Re number at the pipe entrance and the outer pressure, which is denoted as atmospheric pressure.

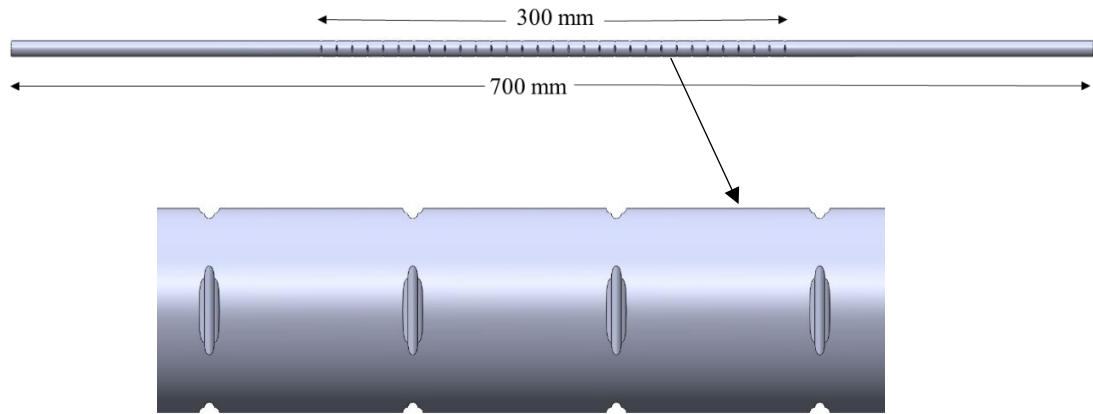


Figure 2: Schematic diagram of doubled dimpled corrugated pipe

#### ***4.1.2 Mesh Configuration***

To capture and illustrate the flow characteristics in pipes, a steady state and three-dimensional model is created using Fluent to generate a computational domain pipe with dimples and corrugations. For numerical calculations, the development of grid domains is an important phase that affects computation time and accuracy. Despite the fact that the flow behavior near the pipe surface is complex in dimpled and corrugated pipes, this region has a significant impact on the pressure drop and Nu number values. The flow generation region is critical to the mesh's computational efficiency as well as its accuracy outcomes.

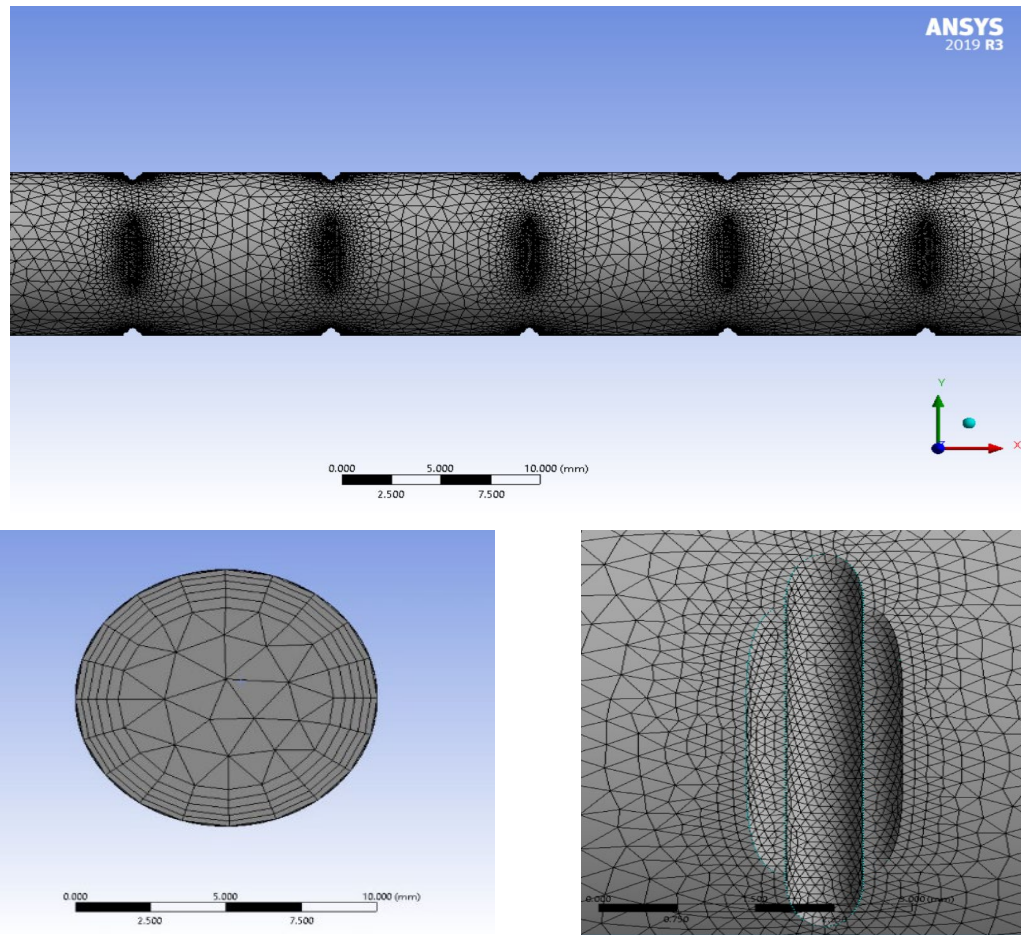


Figure 3: Mesh configuration at the tube's cross section and along its length

Figure 3 illustrates a very fine mesh along the wall and a rather coarse mesh near the centerline. This mesh provided significant convergence results. The computational flow domains are discretized using a structured-tetrahedral mesh because of its advantages in giving more accurate flow calculations. The entire tetrahedral mesh is generated well because of the consideration of a rise in calculation precision and wall functions in the turbulent flow domain, and because of the need to provide evidence of a rise in simulation accuracy.

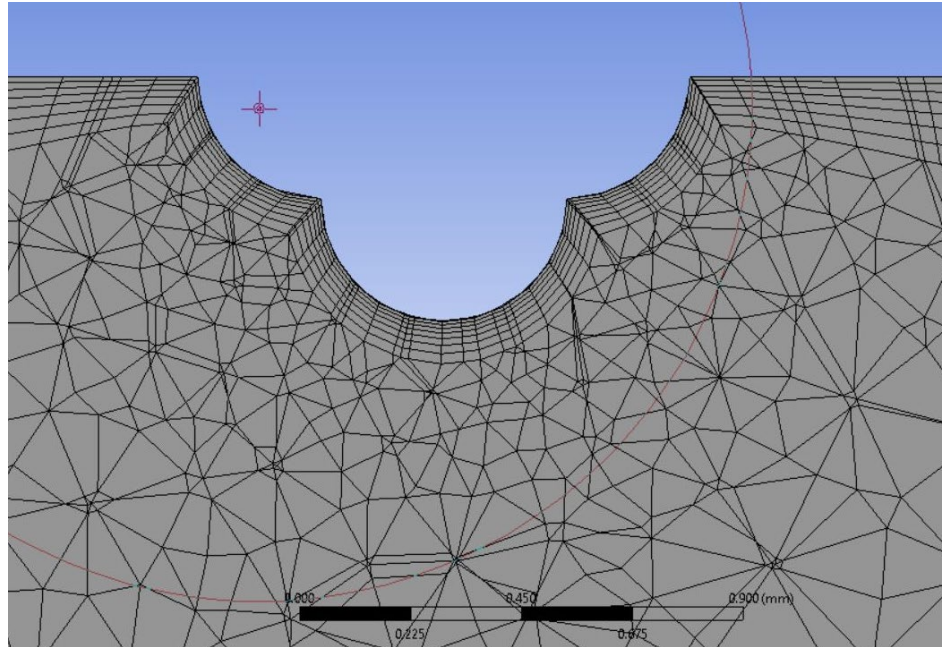


Figure 4: Section plane along the radial direction of the corrugated dimple pipe

In the turbulent flow domain, the inflation layer is an ideal approach for focusing the flow structure near the pipe wall. The inflation layers are constructed to provide precise computation results. Furthermore, several meshes are examined to see how the numerical results affect the results.

#### ***4.1.3 Grid Sensitivity Analysis***

The grid independent analysis is carried out to discover the best mesh quality for accurate numerical calculations with the lowest feasible time consumption. Grid-independent methods were guaranteed by conducting rigorous mesh testing procedures. Corrugated pipe geometry is chosen to be tested with different grid element counts. Nusselt number, velocity, and pressure drop are all taken into account in different element numbers to see whether there are any significant variances with respect to the element numbers.

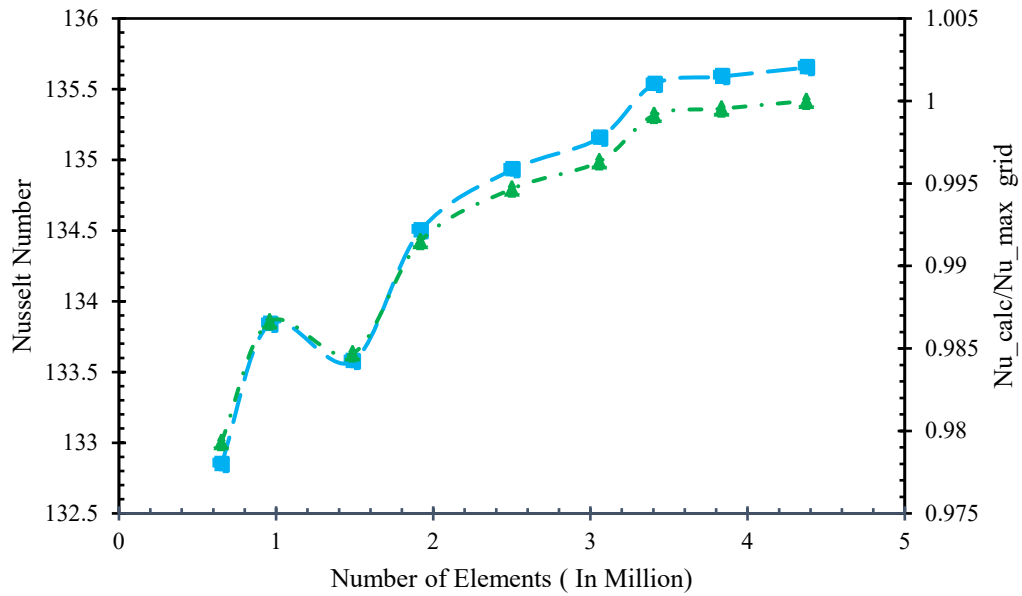


Figure 5: Impact of grid refinement on dimpled pipe

In this study, multiple grid generations are executed when the number of mesh elements ranges from 0.651 million to 4.3 million. The Figure 5 depicts the flow mesh features for dimple pipe. Approximately 3.4 million elements achieve mesh-independent convergence, which is obvious. The 3.4 millionth grid element is chosen for research because its accuracy results are superior to those of previous examples. In terms of saving time and reducing computing expenses, this grid element is chosen for analysis.

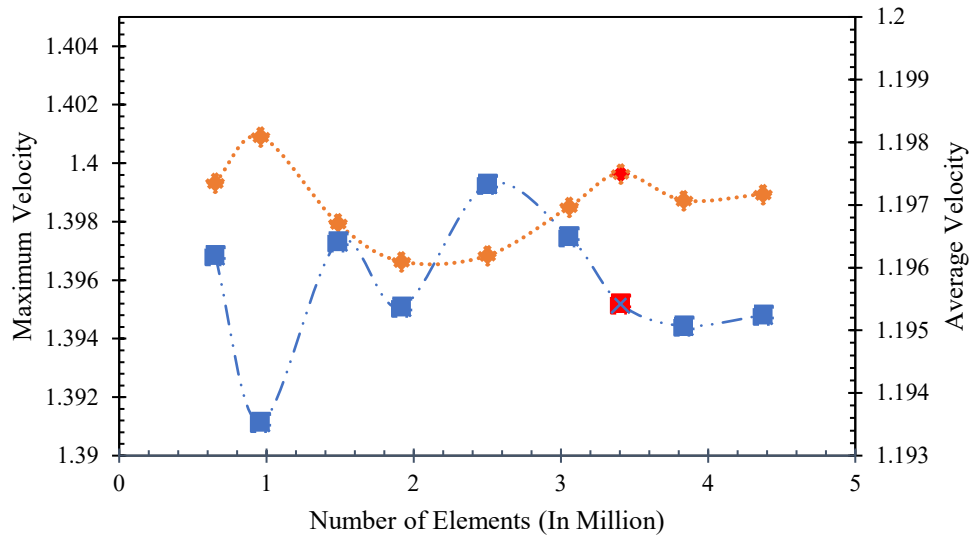


Figure 6: Variation of velocity with varying element size for dimpled pipe at  $Re = 15000$

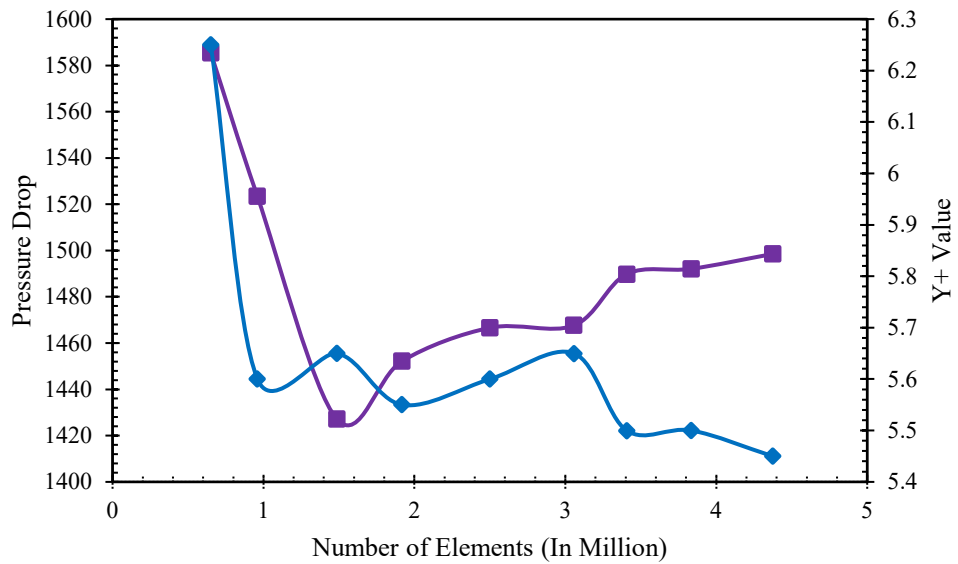


Figure 7: Variation of pressure drop with varying element size for dimpled pipe at  $Re = 15000$



#### 4.1.4 Physical Flow Parameters and Boundary Condition

The inlet conditions are the velocity at the inlet having a 5% turbulence intensity at a fixed temperature (300 K). The output is a pressure outlet condition with a turbulence intensity of 5%. Moreover, the hydraulic pipe diameter is 10 mm. No-slip boundary conditions on the inner and outside walls are based on constant heat flux boundary conditions in the corrugated pipe portions. At Re numbers ranging from 10000 to 30000, the inlet fluid flow is fully developed with a constant inlet velocity. Coupled pressure fields and acceleration speeds can be integrated using 2nd order upwind techniques. These requirements are known as "boundary conditions."

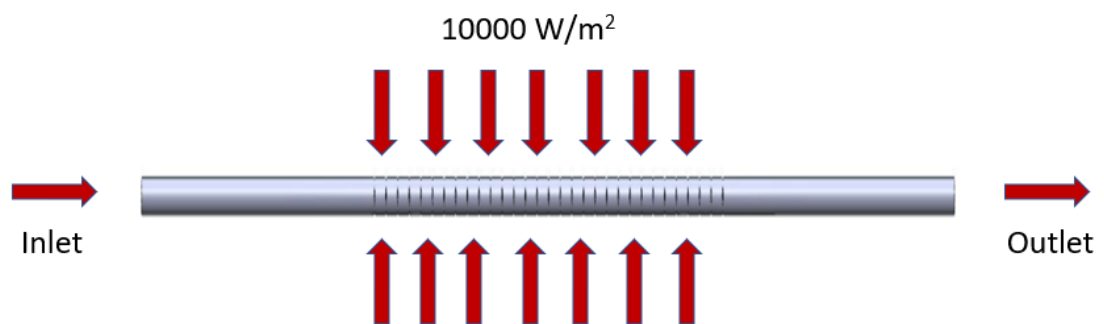


Figure 8: Physical representation of the solution domain

#### 4.1.5 Code Validation

For numerical simulation of turbulent flow in a pipe, it is necessary to validate the accuracy of the current numerical results. An experimental validation of heat transfer performance should be accomplished first to evaluate the numerical system's reliability for flow, pressure drop, and heat performance. An experimental validation by Qi et al.[74] is used to verify the computational results of the corrugated pipes. The numerical results for the corrugated tubes is in agreement with the experimental data, as shown in the figure. The computational model was tested against available experimental data, and some correlations were found as indicated in the following equation. Eqs. (1) and (2) were used to calculate the Nusselt number of water and the friction factor of water, respectively, for validation purposes[75]. According to Eq. (2), the validity ranges of the Dittus-Boelter correlation are  $0.6 \leq Pr \leq 160$ ,  $Re \geq 10000$ , and  $L/D_h > 10$ . [76]

$$Nu = 0.023Re^{0.8}Pr^{0.4} \quad (8)$$

$$f = (0.790\ln Re - 1.64) - 2 \quad (9)$$

Turbulent flow in a corrugated pipe is simulated at Reynolds numbers ranging from 10000 to 30000. First, the numerical results must be validated using Qi et al.[74] experimental data to verify precision. Numerical errors, as measured against experimental data and correlations, ranged from 2 percent to 5 percent. In some cases, fluid characteristics and numerical solutions might lead to this error variation.

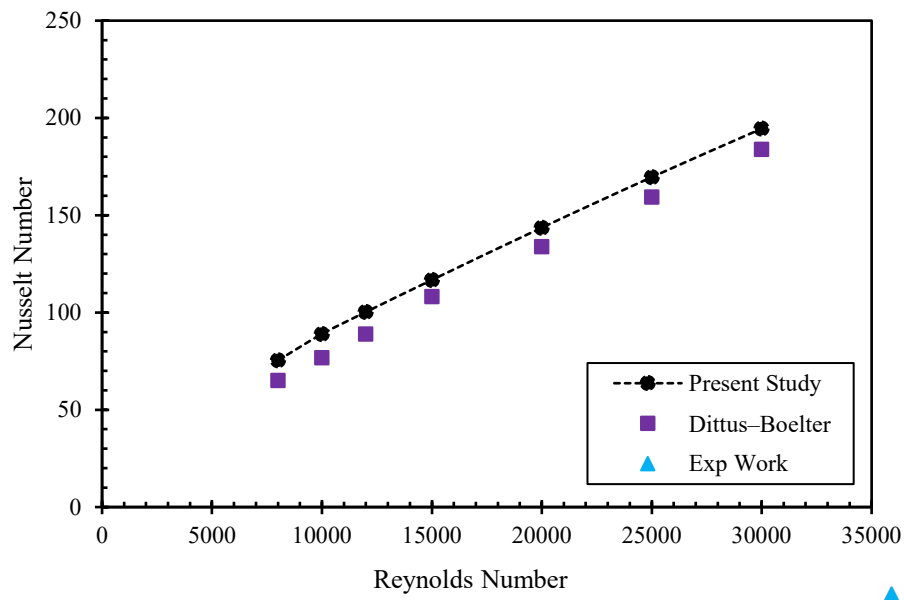


Figure 9: validation of numerical and experimental data in a pipe.

The Nusselt number and computational outcomes appear to be in good agreement when compared numerically and experimentally. Because of this, it can be argued that the existing computational model can accurately forecast the flow and thermal performance of the pipe.

#### 4.1.6 Thermo-Physical Properties of Nanofluids, Water and Nanoparticles

Significant works of literature offering methods to estimate the thermophysical property of nanofluids have been published in recent years. Due to their thermophysical characteristics, the usage of nanofluids in cooling applications has grown. Although nanofluid thermophysical characteristics have been carefully explored, experimental data that is contentious lacks precision. Due to its widespread acceptance in the

literature, a single-phase technique is used for the calculation of thermophysical parameters. The assumption of thermal equilibrium for the particles is made, along with the assumption that the fluid and particles have identical velocities. This hypothesis demonstrates that the correlation of convective heat transfer may also be applied if the nanofluid properties and the thermalphysical property estimated at reference temperatures incorporate. [87]–[90]

Nanofluids with oxide particles larger than 40 nm should be prioritized according to the model presented by Maga et al [91], Effective nanofluid properties can be determined using the following equations:

The density of nanofluids is derived using[92]

$$\rho_{nf} = (1 - \phi)\rho_{bf} + \phi\rho_s \quad (10)$$

The correlation provided by Takabi and Salehi [79] based on the rule of mixtures was utilized to define the density of hybrid nanofluids.

$$\rho_{hnf} = (1 - \phi)\rho_{bf} + \phi_{s,1}\rho_1 + \phi_{s,2}\rho_2 \quad (11)$$

$\phi_{s,1}$  and  $\phi_{s,2}$  are the volume fractions of each nanoparticle in the base fluid, and  $\rho_1$  and  $\rho_2$  are the nanoparticle density. The volume fraction ( $\phi$ ) of nanofluid is added as a new variable.[93]

$$\phi = \frac{V_s}{V_{bf}} \quad (12)$$

Furthermore, the volume fractions of each sort of nanoparticles are specified as follows:

$$\phi_{s,1} = \frac{V_{s,1}}{V_{bf}} \quad (13)$$

$$\phi_{s,2} = \frac{V_{s,2}}{V_{bf}} \quad (14)$$

Nanofluid specific heat capacity is determined by comparing the density, volume fraction and specific heat capacities of the base fluid and nanoparticles.[94]

$$c_{p,nf}\rho_{nf} = (1 - \phi)\rho_{bf}c_{p,bf} + \phi\rho_s c_{p,s} \quad (15)$$

The equation below was used to calculate the hybrid nanofluids' specific heat capacity.[79]

$$c_{p,hnf} = \frac{(1 - \phi)\rho_{bf}c_{p,bf} + \phi_{s,1}\rho_1c_{p,1} + \phi_{s,2}\rho_2c_{p,2}}{\rho_{hnf}} \quad (16)$$

According to the Brinkman equation, the dynamic viscosity of nanofluids can be computed as follows:[95]

$$\mu_{nf} = \frac{\mu_{bf}}{(1 - \phi)^{2.5}} \quad (17)$$

In hybrid nanofluids, the volume percentage of both nanoparticles in the base fluid has been computed as follows using a modified version of the Brinkman equation:[96]

$$\mu_{hnf} = \frac{\mu_f}{(1 - \phi_{s,1})^{2.5} (1 - \phi_{s,2})^{2.5}} \quad (18)$$

The thermal conductivity of nanofluids is computed utilizing the Hamilton–Crosser model [97], a modified version of Maxwell's theory.

$$k_{nf} = k_{bf} \frac{k_s + (n - 1)k_{bf} - \varphi(n - 1)(k_{bf} - k_s)}{k_s + (n - 1)k_{bf} + \varphi(k_{bf} - k_s)} \quad (19)$$

According to this formula, n is a shape factor.

$$n = \frac{3}{\psi} \quad (20)$$

The sphericity of the particles is denoted by  $\psi$ . Nanoparticles with spherical forms have a  $n = 3$  number. [98], [99]

Table 1: Properties of water and nanoparticles

<i>Material</i>	Density, $\rho$ (kg/m <sup>3</sup> )	Heat Capacity, C <sub>p</sub> (J/kgK)	Thermal Conductivity K (W/mK)	Dynamic Viscosity, $\mu$ (kg/ms) $\times 10^{-3}$
H <sub>2</sub> O	995.70	4178	0.615	0.80
Al <sub>2</sub> O <sub>3</sub>	3970	765	40.0	-
CuO	6510	540	18.0	-
TiO <sub>2</sub>	4250	686	8.945	-

Table 2: Thermophysical properties of Al<sub>2</sub>O<sub>3</sub>/water[100][101]

<i>Al<sub>2</sub>O<sub>3</sub>/water</i>	$\phi = 1\%$	$\phi = 2\%$	$\phi = 3\%$
Density (kg/m <sup>3</sup> )	1023.129	1049.15	1101.216
Heat capacity (J/kg K)	4058.87	3944.7	3732.56
Thermal conductivity (W/m K)	0.63	0.648	0.685
Viscosity (Pa.s)	$9.14 \times 10^{-4}$	$9.37 \times 10^{-4}$	$9.87 \times 10^{-4}$

Table 3: Thermophysical properties of CuO/water[102], [103]

<i>CuO/water</i>	$\phi = 1\%$	$\phi = 2\%$	$\phi = 3\%$
Density (kg/m <sup>3</sup> )	1052.129	1107.158	1217.216
Heat capacity (J/kg K)	3953.75	3750.89	3400.2
Thermal conductivity (W/m K)	0.629	0.646	0.681
Viscosity (Pa.s)	$9.14 \times 10^{-4}$	$9.37 \times 10^{-4}$	$9.87 \times 10^{-4}$

Table 4: Thermophysical properties of Al<sub>2</sub>O<sub>3</sub>–CuO/water[104]

<i>Al<sub>2</sub>O<sub>3</sub>–CuO/water</i>	$\phi = 1\%$	$\phi = 2\%$	$\phi = 3\%$
Density (kg/m <sup>3</sup> )	1037.129	1078.158	1159.216
Heat capacity (J/kg K)	4006.75	3847.89	3559.2
Thermal conductivity (W/m K)	0.63	0.648	0.684
Viscosity (Pa.s)	$9.14 \times 10^{-4}$	$9.37 \times 10^{-4}$	$9.87 \times 10^{-4}$

Table 5: Thermophysical properties of Al<sub>2</sub>O<sub>3</sub>–TiO<sub>2</sub>/water

<i>Al<sub>2</sub>O<sub>3</sub>–TiO<sub>2</sub>/water</i>	$\phi = 1\%$	$\phi = 2\%$	$\phi = 3\%$
Density (kg/m <sup>3</sup> )	1011.74	1027.15	1059.86
Heat capacity (J/kg K)	4106.58	4037.40	3905.20
Thermal conductivity (W/m K)	0.623	0.645	0.679
Viscosity (Pa.s)	$12.10 \times 10^{-4}$	$13.02 \times 10^{-4}$	$14.37 \times 10^{-4}$

#### 4.1.7 Data Reduction

For determining the thermophysical characteristics of fluids, the bulk mean temperature of the fluid ( $T_m$ ) is considered.

$$T_m = \frac{T_{in} + T_{out}}{2} \quad (21)$$

Calculating the heat transferred to the fluid through the corrugated pipe,

$$\dot{Q} = \dot{m}c_p(T_{out} - T_{in}) \quad (22)$$

The calculation for the convective heat transfer coefficient was as follows:[99]

$$\dot{Q} = hA_c\Delta T_c \rightarrow h = \frac{\dot{Q}}{A_c\Delta T_c} \quad (23)$$

Based on the hydraulic diameter, the Reynolds number was calculated,

$$Re = \frac{\rho v D_h}{\mu} \quad (24)$$

The performance of convective heat transport can be described by the Nusselt number, a dimensionless parameter. Nusselt number is defined by,

$$Nu = \frac{h_{av} D_h}{k} \quad (25)$$

The following equation includes the friction factor,

$$f = \frac{2\Delta P D}{\rho v^2 L} \quad (26)$$

The following equation was used to compute the pressure drop ( $\Delta P$ ) for the flow characteristics of nanofluids,

$$\Delta P = P_{in} - P_{out} \quad (27)$$

The equation for the performance evaluation criterion (PEC) is as follows,[105]

$$PEC = \frac{Nu_{enhanced} / Nu_{bf}}{(f_{enhanced} / f_{bf})^{1/3}} \quad (28)$$

## 4.1.8 Flow Behavior Investigations

### 4.1.8.1 Pressure Distribution

Fluctuations in static pressure within the corrugated pipe are observed in Figure 10 when the pipe's corrugation ring is fully extended. The inlet temperature is 300K, the inlet velocity is 1.99 m/s, and the Re number is 25000 with a constant heat flux of 10000 w/m<sup>2</sup>. As the length of the corrugated test pipe extends, the pressure declines. There are also varying levels of pressure. According to this diagram, pressure is higher near the inlet and lower towards the output of a pipe. After that, the positive pressure gradient at the increased flow parts can be seen. In addition, the friction factor in pipe will significantly raise more than in smooth pipe based on the preceding calculations.

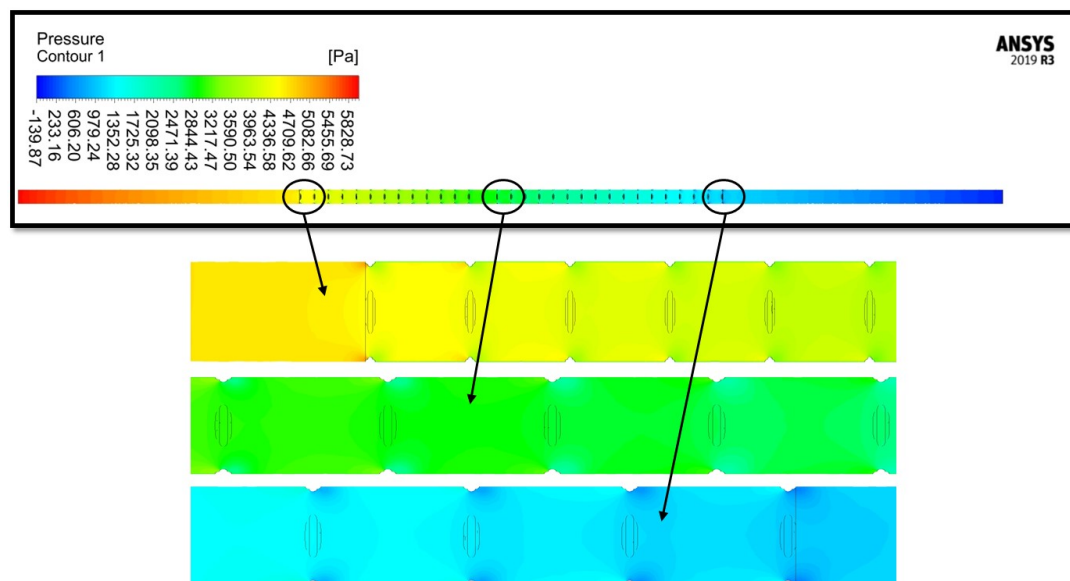


Figure 10: Pressure distribution in a corrugated test section from several positions

The pipe core showed the highest value in the dynamic pressure region, indicating the presence of a circulation zone. Due to the low velocity in this region, the lowest pressure readings were observed close to the pipe walls. Disrupting the flow stability by using passive techniques like corrugation, dimples, and twisted tape can lead to more variation in streamlines flow. Dynamic pressure changes and increased heat performance are both enhanced by these distorted flow zones between passive devices and the flow inside the pipe. [106]



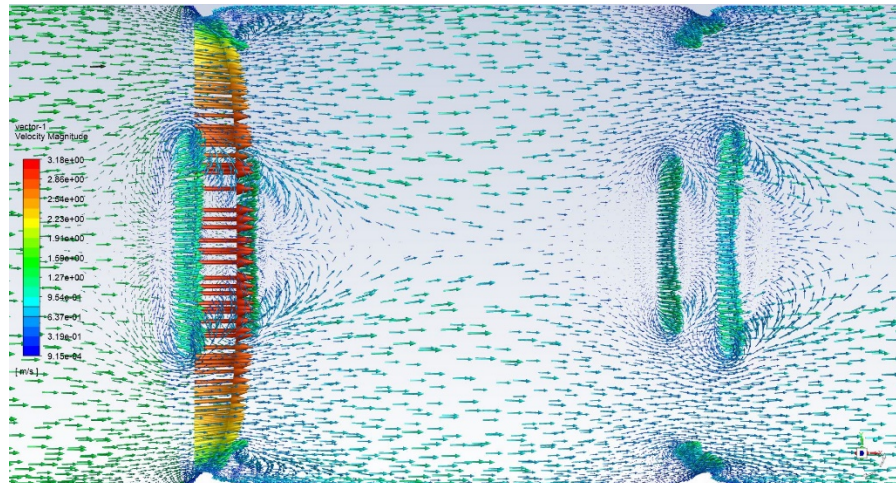


Figure 11: Swirl flow at the corrugated dimpled section

Figure 11 clearly shows that these geometrical arrangements have a significant impact on the flow field in terms of (a) dynamic pressure and (b) velocity magnitude parameter contours. It has been discovered that the corrugated dimples has a significant impact on both variables. Corrugated pipes have an inflow tendency that is periodic due to the fluctuations in dynamic pressure and velocity. Corrugated rings cause a fluctuation in flow field, with the lowest pressure and velocity values occurring close to the corrugated wall.

#### 4.1.8.2 Variation in Flow Velocity

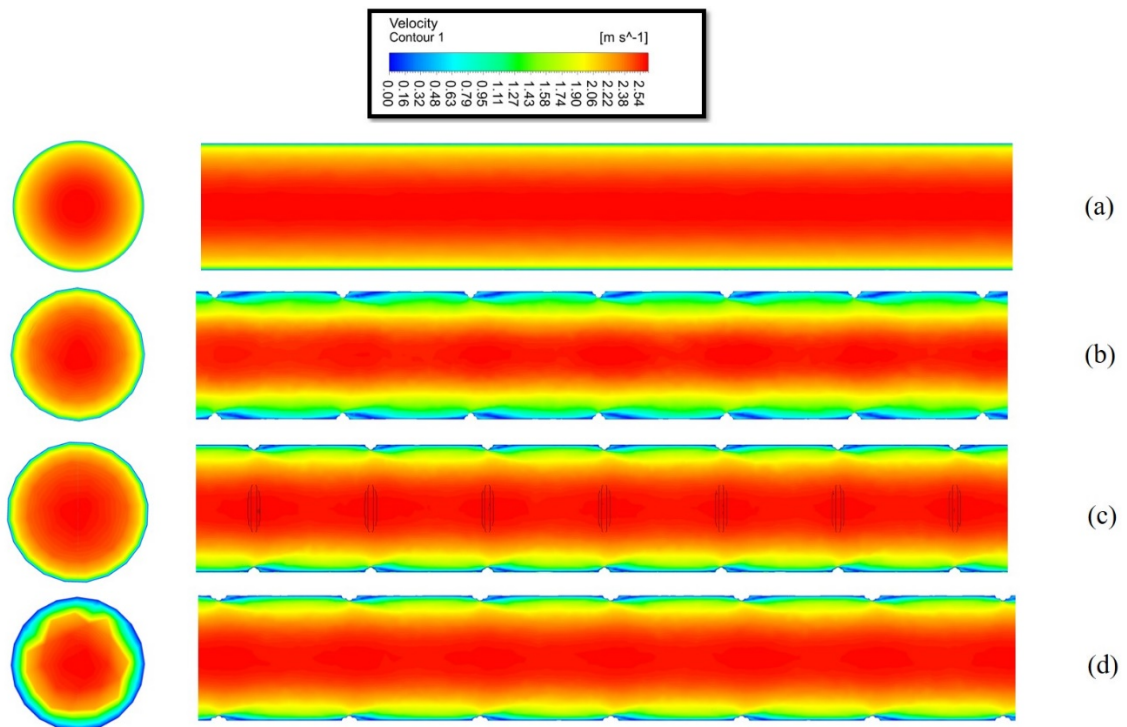


Figure 12: Variation in flow velocity in smooth and dimpled pipes (a) smooth pipe, (b) aspect ratio of dimpled configurations 2, (c) aspect ratio 2.5, (d) aspect ratio 3

Figure 12 shows the velocity measurement outlines. One must clearly show how strong the flow is when it is viewed from the primary flow direction. At the pipe's outside edge, dimple designs promote mixing, secondary flow and swirl flow strength. Swirl flow zone size is found to be dependent on pipe wall dimple's diameters and dimple arrangement, and this was found to be a function of both. It has also been found that increasing the concavity diameter leads to an increase in velocity. Increasing the number of passive devices in pipes can lead to a greater circulation area, which results in more vortices. This passive device (dimples) improves swirl flow in pipes, which leads to greater secondary flow and, consequently, more turbulent mixing and higher heat performance. As a result of this interaction, more impinging streams can be generated, which in turn improves fluid mixing and, as a result, increases the heat transfer between the pipe interior and the wall. Improved heat transmission via recirculation fluid is made possible by creating impinging streams in the pipe.[107], [108]

Disrupting the flow within that thermal boundary layer is made more difficult by the presence of various passive devices in a pipe. As a result, the increase in the temperature difference between the fluid and the surrounding air. There are numerous geometrical configurations that affect heat performance, as shown by Figure . Compared to a smooth pipe, the temperature in pipes increases as the dimple diameter increases. These findings demonstrate that all these layouts have significant impact on heat transfer. The overall heat output can be improved because of these temperature changes. As a result, the pipe's thermal boundary layer thickened, resulting in a greater effect on rotation and flow mixing from dimples, twisted tape inserts, and corrugated sections.[109]

#### 4.1.8.3 Temperature Contour

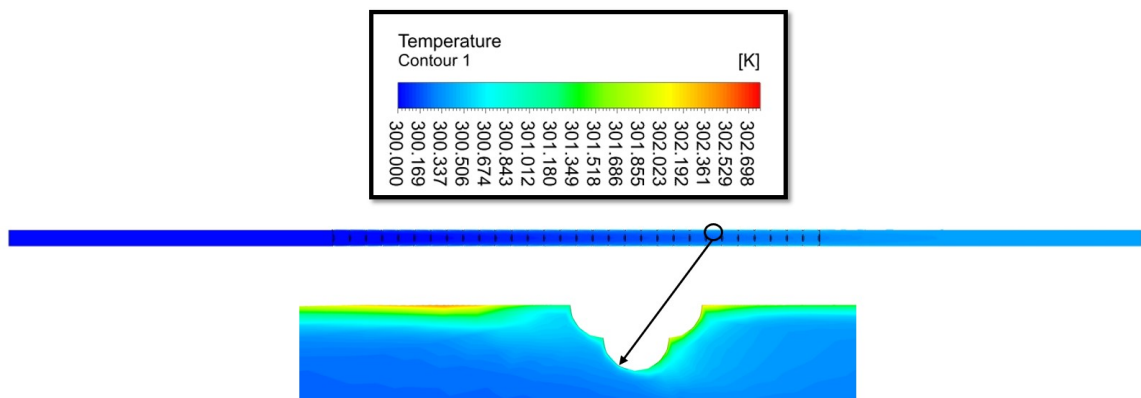


Figure 13: Temperature variations in dimpled corrugated pipe

A change in temperature can be observed as the pipe length increases, with the higher temperature reaching 302 K. Corrugated surfaces can cause flow patterns to be disrupted due to flow mixing, secondary flow, and swirl flow being used.[110]–[112]

#### 4.1.9 Effect of Geometry

##### 4.1.9.1 Heat Transfer Performance Analysis

The Nusselt number of several configurations of corrugated pipe is represented in the figure. As shown in the , the aspect ratio of 2 has superior heat transfer performance. At a Reynolds number of 20,000, the Nusselt number of Al<sub>2</sub>O<sub>3</sub> nanofluid is 144.7569126, 168.2277658, 162.1025263, and 158.3362038, respectively, for simple,

aspect ratios of 2, 2.5, and 3. Depending on the Reynolds and Prandtl numbers as well as the corrugated channel aspect ratios, the results demonstrated that the mixing produced by these self-sustaining transverse swirls considerably improves heat transfer.

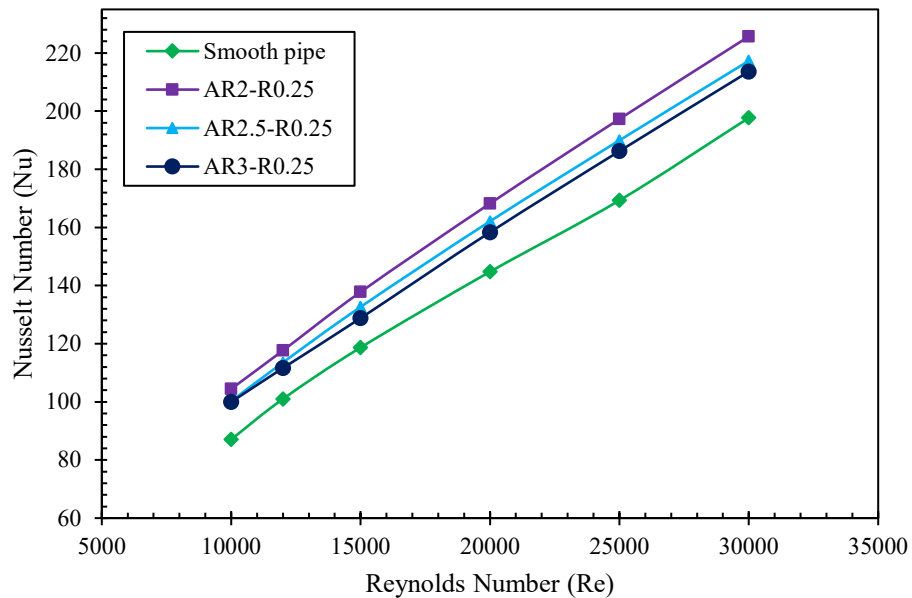


Figure 14: Variation of Nusselt number with Reynolds number for different geometries

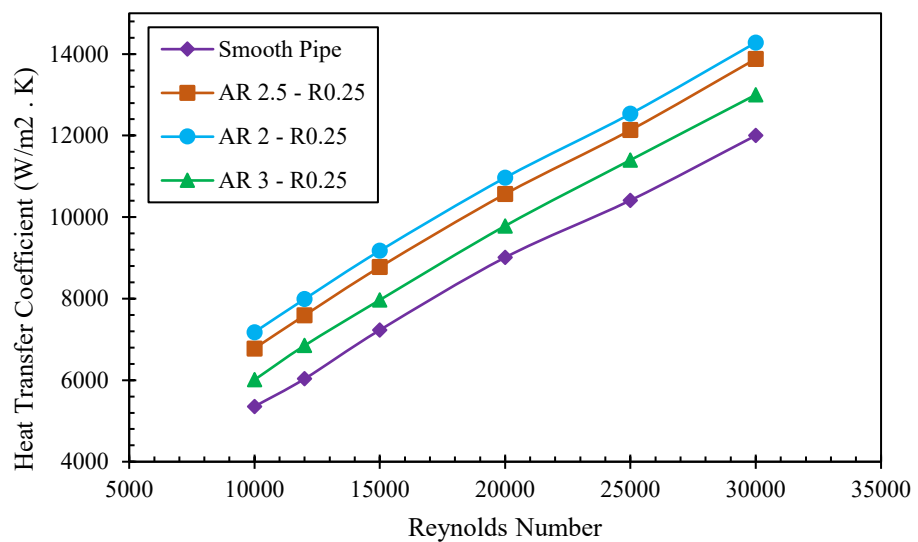


Figure 15: Variation of convective heat transfer coefficient with Re for different geometries

Due to the decreased cross-sectional area and hydraulic diameter, the inlet velocity of a corrugated pipe increases as the aspect ratio decreases. A structure with a smooth curve that permits particles to interact and transfer heat and energy uniformly, whereas corrugated pipes have sharp edges that can impede the flow and hence reduce the fluid's heat transmission capability. It is suggested that the bulk flow field inhibits the flow near the jagged corners (or vertices) of the corrugated pipes due to its higher velocity. [113]

#### 4.1.10 Pressure Drop

Figure 16 depicts the decrease in pressure of Al<sub>2</sub>O<sub>3</sub>/H<sub>2</sub>O nanofluids with various geometries. It is evident from Figure that the pressure drop of nanofluid in a corrugation design with an aspect ratio of 2 is greater than that of other corrugation configurations. The pressure drop across the corrugated pipe of AR 2 for 1% Al<sub>2</sub>O<sub>3</sub>/H<sub>2</sub>O nanofluid is 2524 kPa at a Reynolds number of 20000, whereas it is 1910 kPa, 1900 kPa, and 1110 kPa for the other design at the same Reynolds number and composition.

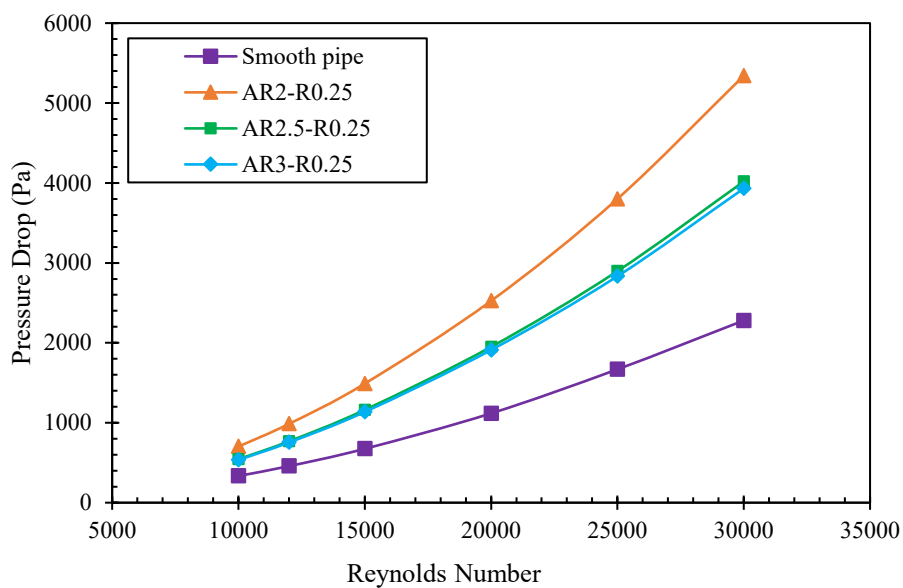


Figure 16: Pressure drop of 1% Al<sub>2</sub>O<sub>3</sub>/H<sub>2</sub>O nanofluid in different geometries

Due to the high wall shear stress, the aspect ratio of 2 experiences a substantial pressure drop. The high wall shear stress is caused by the strong velocity gradient near the wall [29]. In addition, as the Reynolds number rises, the difference in pressure drop across the investigated geometries becomes more significant. As mentioned, this is because the nanofluid's pressure drop increases as the Reynolds number increases.[114]

This work investigates the evaluation of pressure drop to improve thermal efficiency. In comparison to the smooth channel, the pressure loss in the dimpled channel is greater due to changes in the velocity profile and turbulence caused by the dimpled portions. With increasing volume fraction, a larger pressure drop is observed due to the increased density and viscosity.[115], [116]

#### 4.1.11 Shear Stress

Due to the increase in viscosity as concentration increases, nanofluids experience an increase in pressure drop. This increases wall shear stress as fluid viscosity increases [Figure 17](#). A greater pressure drop is indicated by higher wall shear stress. When it comes to nanofluids, it can be observed that the pressure drop enhancement diminishes as the Reynolds number increases.[117]

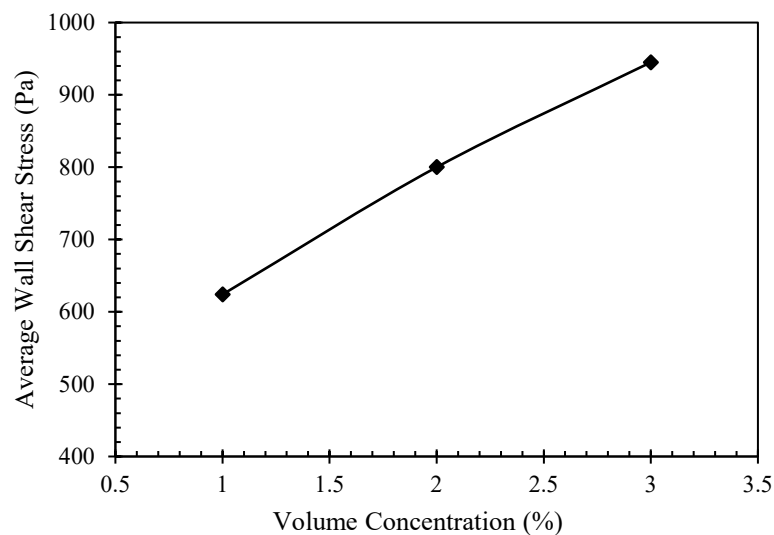


Figure 17: Wall shear stress of Al<sub>2</sub>O<sub>3</sub>/H<sub>2</sub>O nanofluid in corrugated pipe of AR 2 at Re= 20000

When the Reynolds number rises, the temperature and velocity boundary layer thickness decreases, which limits the resistive effect of the nanofluid as it passes through the pipe. [118]

#### 4.1.12 Entropy Generation

Bianco et al. [119] regard the entropy generation analysis to be an efficient technique for investigating and enhancing thermal design [120]. By lessening it, optimum working conditions can be obtained. Typically, the creation of entropy signifies the irreversibility of a system. By minimizing it, a more efficient system has been developed. According to Refs. [120][121], reduction of entropy generation is a well-established method for enhancing a thermal performance. When working with nanofluids, it is also crucial to establish the ideal concentration to employ and the most practical particle size to consider.[122] Consequently, entropy generation analysis provides a rigorous physical foundation for addressing the aforementioned issues (Bianco et al. [119]).

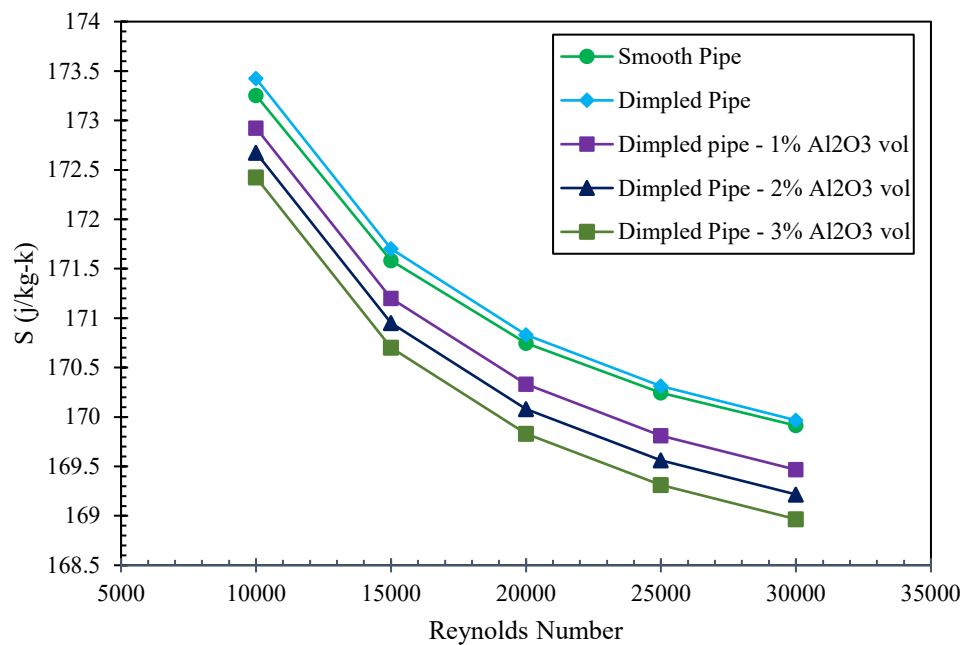


Figure 18: Variation in volumetric entropy generation for Al<sub>2</sub>O<sub>3</sub>/water

Figure 18 demonstrates the variation in volumetric entropy generation as a function of  $Re$  for various coolants. A reduction in volumetric entropy generation with increasing  $Re$  may be observed in the figure, as dimpled channels generate more than smooth ones. The figure shows that the volumetric entropy generation for the dimpled channel falls as the volume percentage of nanofluid increases, with the lowest value found at 3 percent volume concentration of nanofluid. Nanofluids' volumetric entropy generation decreases as volume fraction increases, according to the observations. The addition of nanoparticles could explain the observed changes in the above result, such as an increase in heat conductivity.

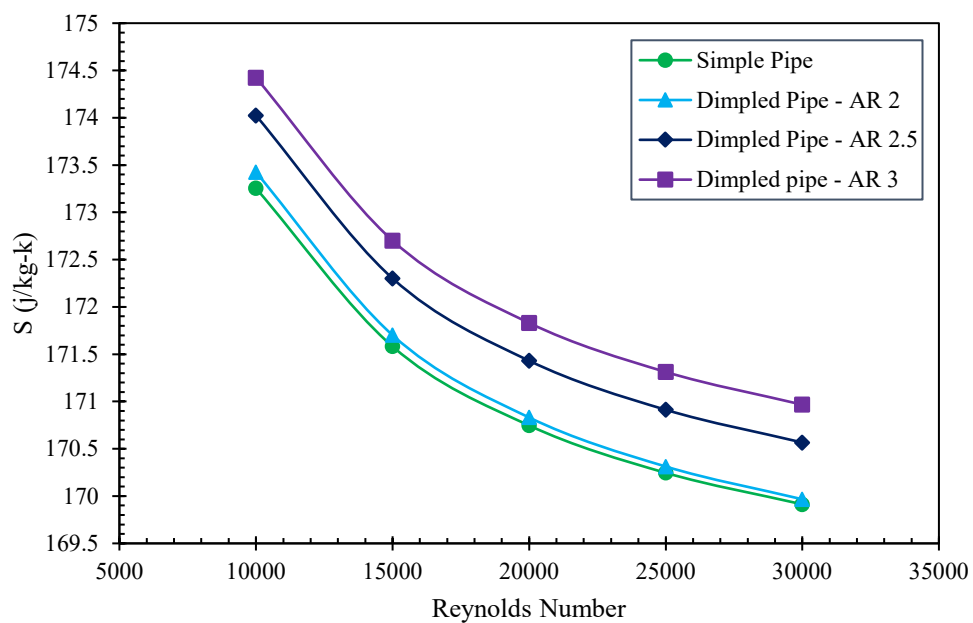


Figure 19: Variation in volumetric entropy generation for different corrugation configurations for 1%  $Al_2O_3$ /water

For  $Al_2O_3$ /water nanofluids with the same volume percent, the entropy generation with  $Re$  is shown in Figure 19. Analyzing the thermophysical characteristics of individual nanofluids is the goal of this work. As shown in Figure the largest entropy generation is found in the aspect ratio of 3 while the lowest entropy generation is found in aspect ratio of 2. Decreasing the aspect ratio enhances the optimum thermal design condition by reducing entropy generation.



#### 4.1.13 Performance Evaluation Criterion

Using nanofluid in corrugated tubes dramatically improves heat transfer, as demonstrated in the previous section. A bigger pressure drop across the tubes, especially when using nanofluid with high volume concentration, is required to achieve this. Nanofluid's prospective advantage in heat transfer may be hindered by the penalty of greater pressure drop; hence, it has to be evaluated for thermal performance. When considering the heat transfer performance of nanofluid, performance evaluation criteria (PEC) are employed to see if it can overcome the higher-pressure drop penalty. The PEC can be calculated from Eq. by dividing the effect of increased heat transfer by the increase in friction factor (eqn 28). Nanofluids with PEC ratios greater than 1 suggest that fluid heat transfer performance dominates that of air resistance since the PEC ratios of water at various Reynolds numbers are equal to one. When compared to water, this suggests a higher thermal conductivity value. [123]

Table 6: PEC of Al<sub>2</sub>O<sub>3</sub>-H<sub>2</sub>O nanofluid in different configurations

Aspect Ratio	Reynolds Number	PEC
2	10000	1.3
	15000	1.15
	20000	1
	25000	0.9
	30000	0.85
2.5	10000	1.2
	15000	1.05
	20000	0.95
	25000	0.86
	30000	0.81
3	10000	1.1
	15000	1
	20000	0.9
	25000	0.8
	30000	0.76

The relationship between the dimple's aspect ratio and the  $Nu/Nu_0$  ratio has been observed in the figure. An evaluation factor (PEC) for three corrugated configuration is shown in that figure. A reduction in PEC is observed as the aspect ratio increases; the best thermal performance is achieved at a  $Re$  of 10000 by using aspect ratio of two. [124]

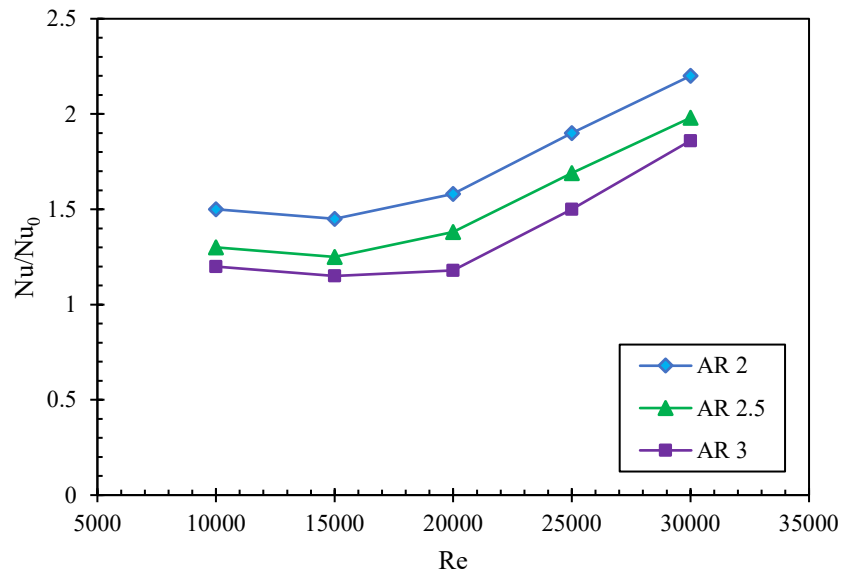


Figure 20: Variations in  $Nu/Nu_0$  and with Reynolds Number

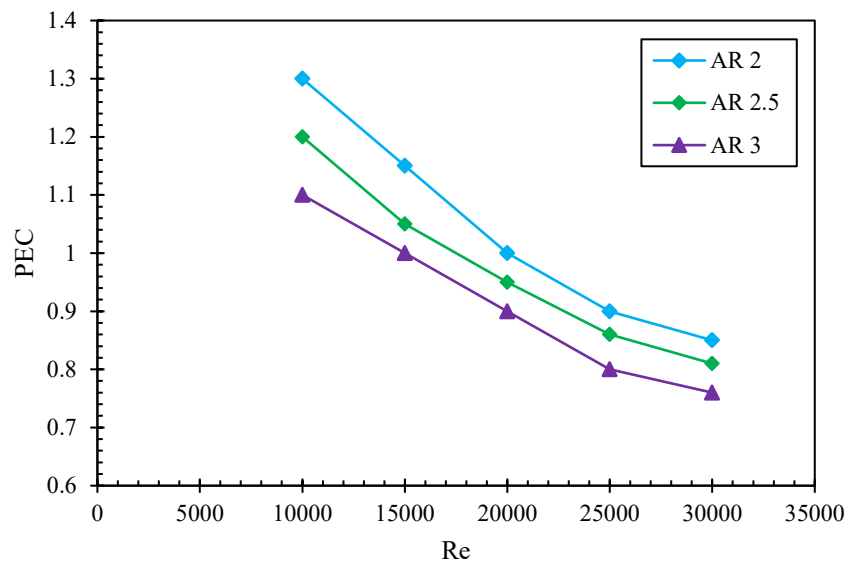


Figure 21: Variations in PEC with Reynolds Number

The PEC value decreases as the volume fraction of each nanofluid increases. Density and pressure will decrease because of this circumstance. As a result, for the current dimpled test section, the PEC value drops as the volume fraction increases.

## 4.2 Different Corrugated Channels

### 4.2.1 Description of Computational Domain

#### 4.2.1.1 Trapezoidal Fluid Domain

There are three values of amplitude-wavelength ratios: 0.08, 0.1, and 0.12. The working fluid is considered to circulate through the trapezoidal-shaped fluid domain. Figure 1 depicts the fluid domain's geometry for reference. The flow of the nanofluid through the channel is described as a single phase flow in the simulation software. The inlet velocity is considered to remain constant, and the Reynolds number is used to estimate it.

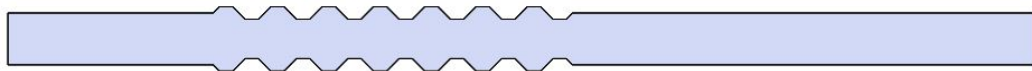


Figure 22: Geometry of the trapezoidal fluid domain

#### 4.2.1.2 Sine Shaped Corrugated Fluid Domain

An incompressible fluid is subjected to turbulent flow in sine shaped corrugated tubes in this experiment. According to the diagram in the figure 3, the present study's geometry and its many parameters are carried out.



Figure 23: Geometry of the sine shaped fluid domain

### 4.2.1.3 V-corrugated Fluid Domain

Three distinct amplitude values are used to alter the amplitude-wavelength ratio (2 mm, 2.5 mm and 3 mm). A constant 25 mm channel height has been used.

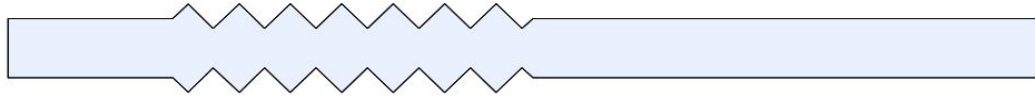


Figure 24: Geometry of the V-shaped fluid domain

### 4.2.2 Mesh Configuration

zStructured mesh has been utilized to discretize the computational flow domains. Because of this mesh, double indices ( $i, j$ ) in two dimensions or triple indices ( $i, j, k$ ) in three dimensions can be used to conveniently address the points of an elemental cell. The interconnectivity is obvious since the indices identify cells adjacent to a certain elemental face, and the cell edges form a continuous mesh line that begins and ends the opposite elemental face. Structured meshes enable for easy data management and regular coupling, which makes task easier.

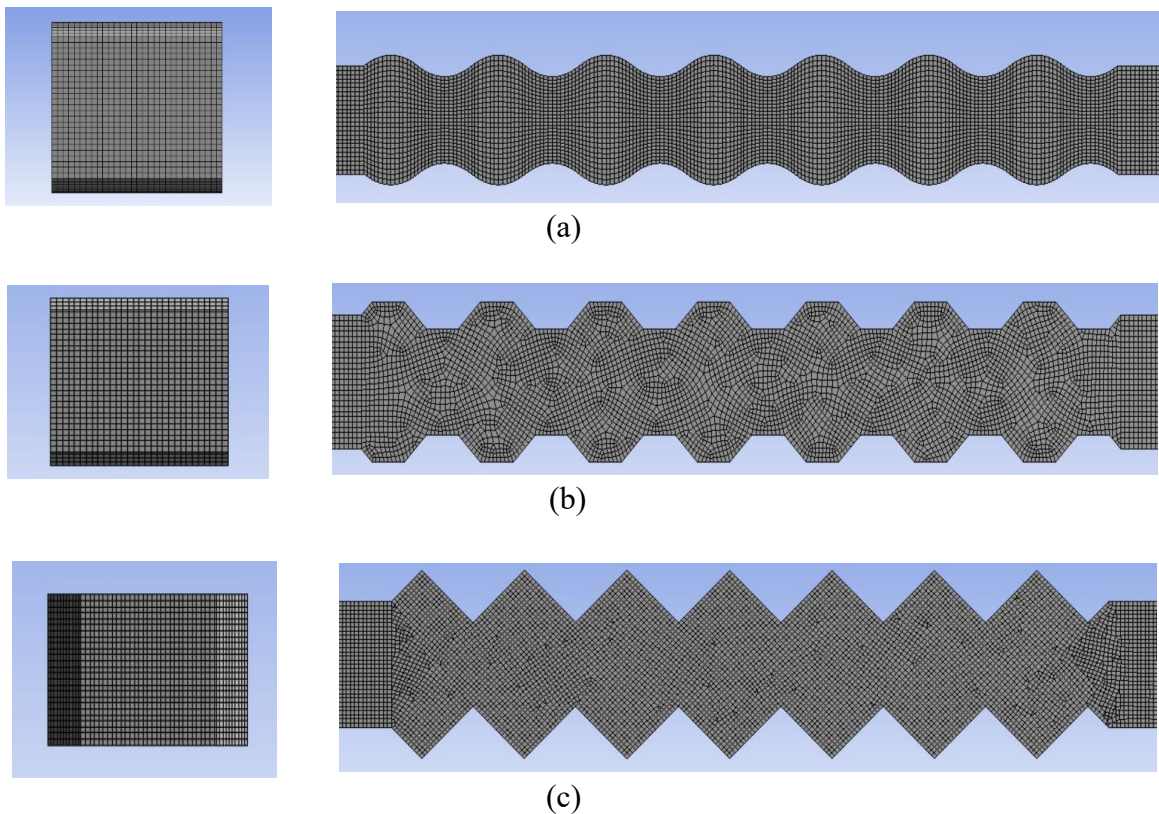


Figure 25: Mesh configuration at different corrugated channel's cross section and along its length (a) sine shaped, (b) trapezoidal, (c) V-shaped

### 4.2.3 Grid Sensitivity Analysis

Using a grid independence test, we have been able to determine the ideal fluid domain grid size for this investigation. The average Nusselt number at the corrugated surface of the trapezoidal channel has been investigated with various grid sizes.

Beyond a grid size of 3 million, the Nusselt number does not vary significantly. As a result, all of the simulations in this work were run on a 3 million nodes layout. Both the V corrugated channel and the rectangular corrugated channel have shown similar results. That is why we have chosen the same amount of grids to represent each geometry.

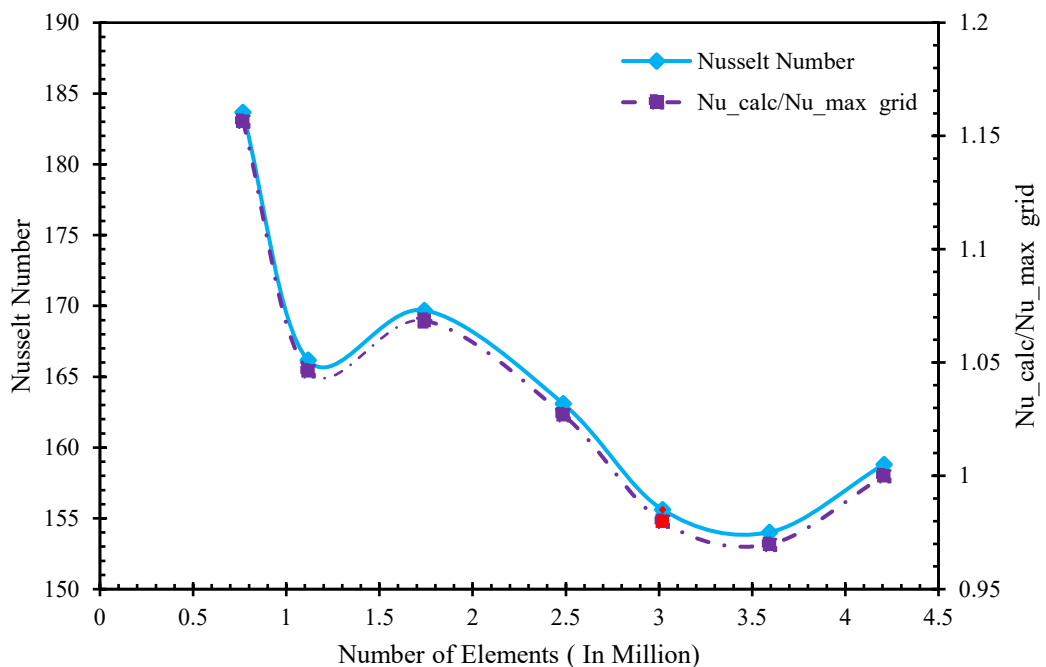


Figure 26: Variation of Nusselt Number with varying element size for trapezoidal channel at  $Re = 15000$

#### 4.2.4 Physical Flow Parameters and Boundary Condition

The inlet circumstances are an inlet velocity with a 5% turbulence intensity at a constant temperature (300 K). The output is a pressure outlet condition with a five percent turbulence intensity. In addition, the diameter of the hydraulic pipe is 10 mm. Internal and external no-slip boundary criteria are based on constant heat flux boundary conditions in the corrugated pipe sections. At Re values between 10000 and 30000, the inlet fluid flow is fully developed at a steady velocity. Using second order upwind approaches, it is possible to integrate coupled pressure fields and acceleration speeds. These conditions are referred to as "boundary conditions."

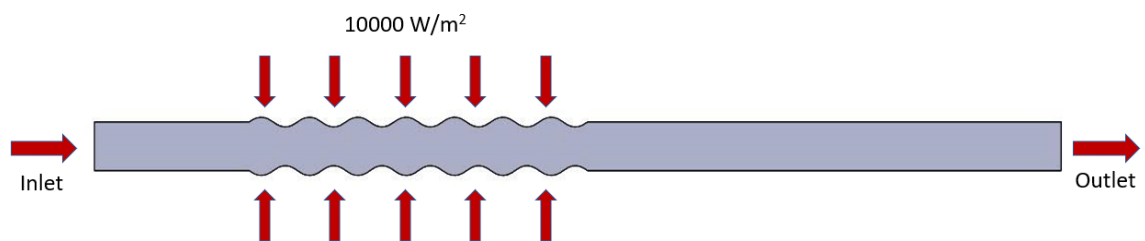


Figure 27: The solution domain as a representation of its physical state

#### 4.2.5 Code Validation

For validation reasons, equations (1) and (2) were used to calculate the Nusselt number and friction factor of water, respectively. The validity ranges of the Dittus-Boelter correlation, according to Eq. (2), are  $0.6 \leq Pr \leq 160$ ,  $Re \geq 10000$ , and  $L/D_h > 10$ . Numerically comparing the Nusselt number and computational results reveals a high degree of congruence.

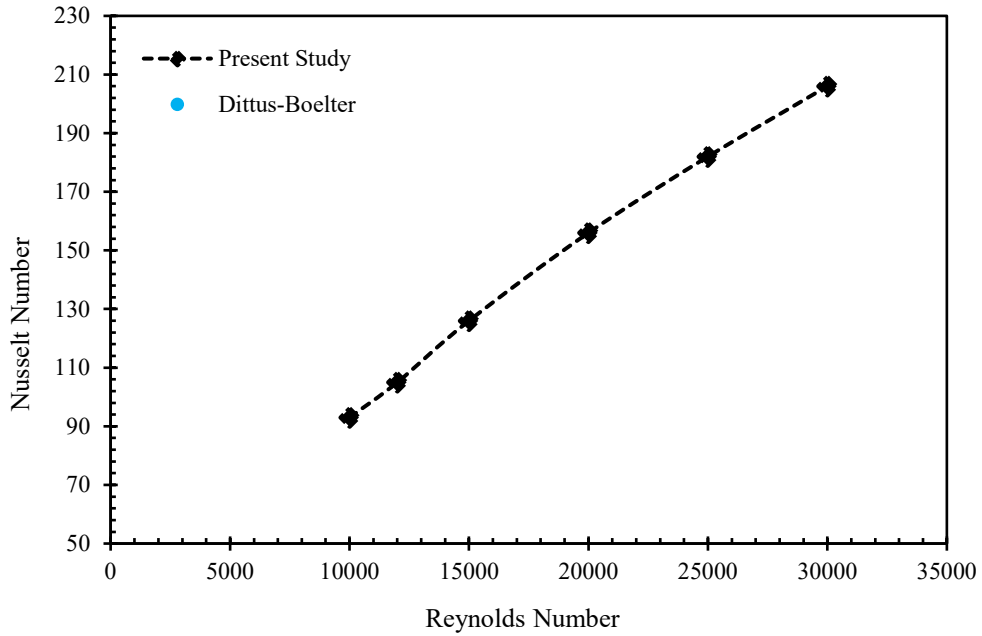
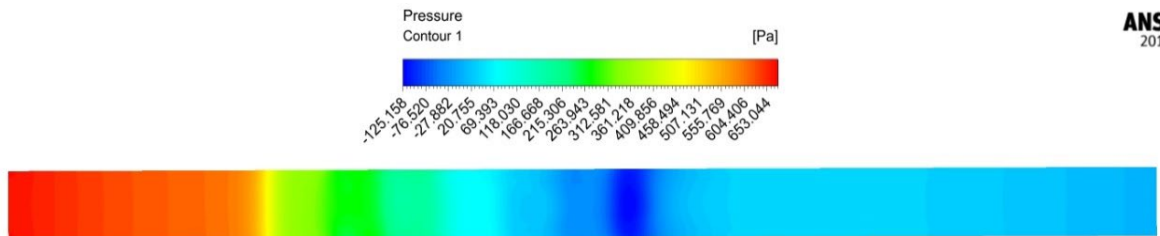


Figure 28: validation of numerical data in a corrugated channel

It can therefore be argued that the existing computer model can accurately predict the pipe's flow and thermal performance. As evaluated by correlations, numerical errors ranged between 2 and 5 percent. In certain instances, fluid properties and numerical solutions may contribute to this error variance.

#### 4.2.6 Flow Behavior Investigations

##### 4.2.6.1 Pressure distribution



(a)

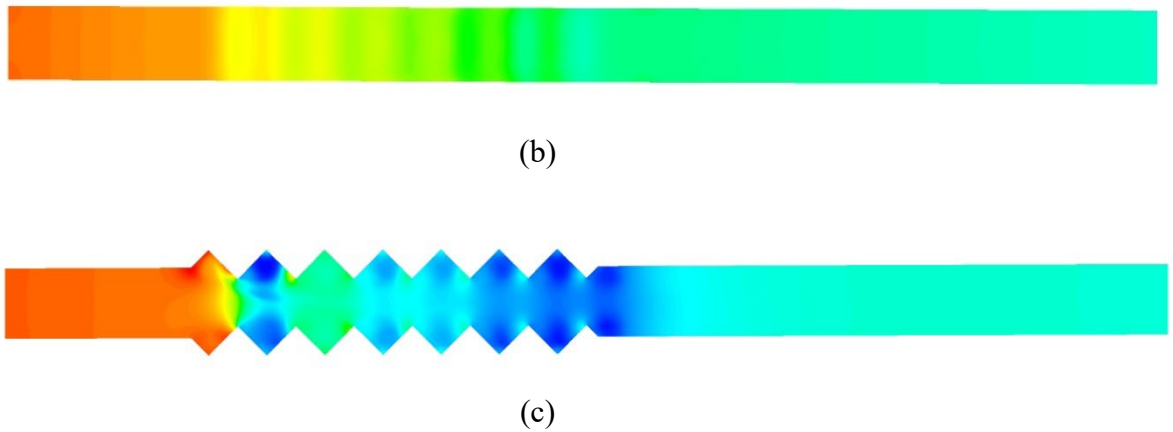
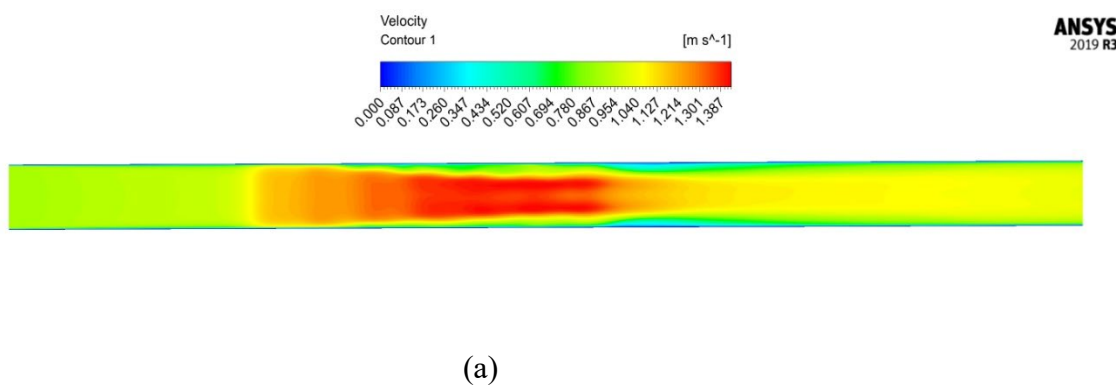


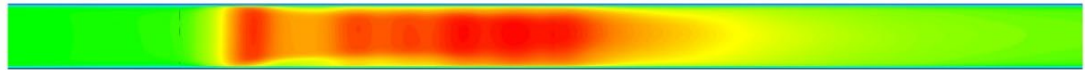
Figure 29: Pressure drop across (a) trapezoid, (b) sine-shaped, (c) V-shaped corrugated section

Because of the strength of the re-circulation zone, the trapezoidal-corrugated channel had the largest pressure decrease at any amplitude. Another reason why trapezoidal-corrugated channels have a higher-pressure drop is that they have a bigger throat area than other channel designs, which has a large wall surface area. The channel shape influence on the pressure drop at  $Re = 10,000$  of water is not evident and is relatively near to each other because the flow is less disturbed at low  $Re$ . This means that the pressure drop in the straight channel is predicted to be the lowest because of its consistent flow and absence of re-circulation zones.

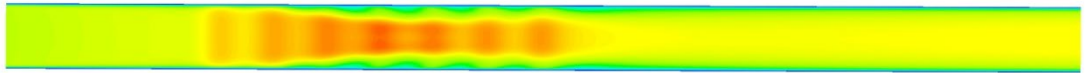
#### 4.2.6.2 Variation in flow velocity







(b)



(c)

Figure 30: Variation in flow velocity in (a) trapezoid, (b) sine-shaped and (c) V-shaped corrugated channel

A rise in the velocity of the opposing flow has been a sign that it was becoming more disturbed and that it was expanding at the expense of the primary flow. As a result, the thermal boundary layer is reduced at high  $Re$  because the recirculation flow efficiently blends a hot fluid near corrugated surfaces with a cold fluid in the middle of the channel. Among the many types of channels, the trapezoidal corrugated one had the most recirculation zones, followed by semicircle, house, and straight ones.

The recirculation zones emerge in the trough of the corrugated walls and increase with increasing  $Re$ . Accordingly, the corrugated walls' wrinkling caused an unfavorable flow that flowed the opposite direction as the main flow.

#### ***4.2.6.3 Temperature contours***

As discussed with different corrugated channel, the figure 14 graph illustrates how the form of the corrugated channel affects the isotherm contours as a function of  $Re$ . Due to the top and bottom walls of the corrugated channels being asymmetrical; the centerline of the channel is symmetrical in terms of velocity and temperature contours.

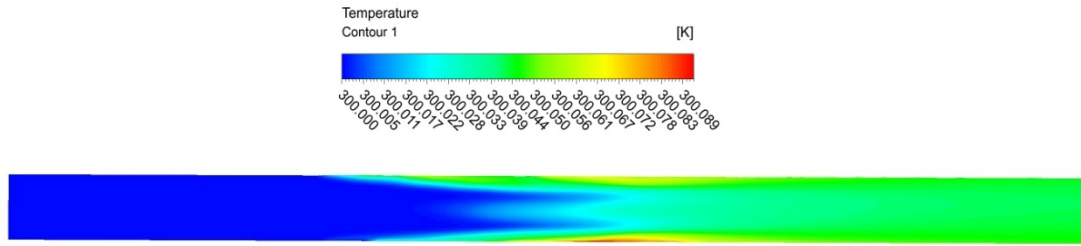


Figure 31: Temperature contours in trapezoidal corrugated channel

By mixing the opposing flow, which is in contact with channel walls, with that flowing through the channel's center, the temperature contours show how corrugated surface and Reynolds number affect temperature gradients near corrugated walls. In addition, as  $Re$  increased, the temperature gradients increased as well.

#### 4.2.7 *Effect of Geometry*

##### 4.2.7.1 *Heat Transfer Performance Analysis*

In this section, the influence of corrugated channels on the  $Nu$  and  $p$  values has been examined using pure water. In all circumstances, as seen in Figure 5, the  $Nu$  rises as  $Re$  rises. When comparing the corrugated channels, it is possible to see a significant improvement in  $Nu$  by raising the coolant's mass flow rate ( $Re$ ). At a specific  $Re$ , both trapezoidal and sine-corrugated channels were found to have a higher  $Nu$  than smooth pipes. In this situation, the real reasons are the growth of secondary flows and the creation of secondary flows, and the intensity of the flows is dependent first on the geometric model and then on the qualities of the coolant. The effect in this example is dependent on the channel configuration because all of the findings are centered on the same fluid.

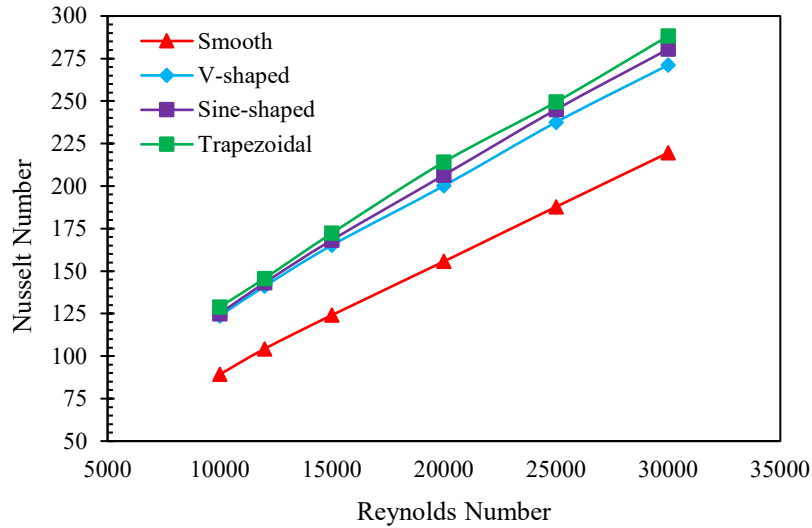


Figure 32: Variation of Nusselt number with Reynolds number for different geometries

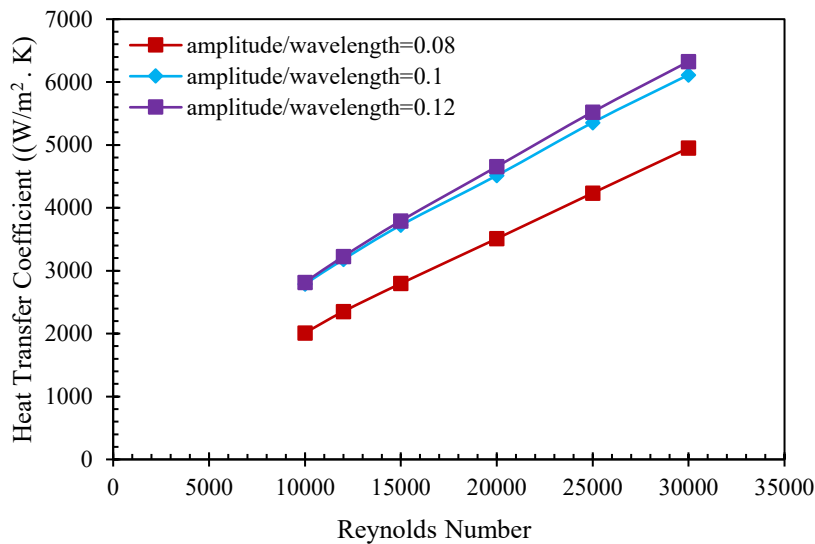


Figure 33: Variation of convective heat transfer coefficient with Re for different geometries

For several amplitude-wavelength ratios, such as 0.08, 0.10, and 0.12, the convective heat transfer coefficient at the corrugated surface is shown in the figure. The heat transfer coefficient increases as the value of rises. While at lower Reynolds numbers, this effect is smaller, it is bigger at higher Reynolds numbers. A Reynolds number of 30000 results in an increase in the value of "h" of 20.5 percent when using  $\alpha= 0.12$  instead of  $\alpha= 0.08$ .

#### 4.2.7.2 Pressure Drop

For demonstration purposes, determining the  $p$  for the flow associated with friction loss can be used to determine hydraulic performance. The figure shows the  $\Delta p$  in each of the examined channels. The  $\Delta p$  increased with the usage of corrugated channels as opposed to smooth pipes. Along with an increase in surface area, the blending factor also contributed to an increase in pressure.

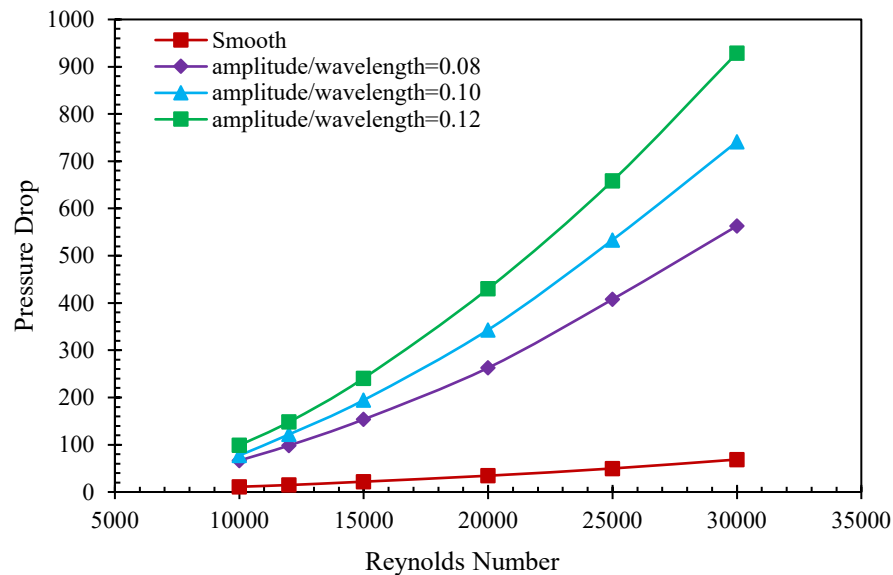


Figure 34: Pressure drop in different geometries

It is shown in Figure 34 that the observed channels pressure drop ratio to the pure water flow ratio in the smooth pipe is more than one. With a rise in the  $Re$ , the pressure drop ratio decreases in all channels.

#### 4.2.7.3 Performance Evaluation Criterion (PEC)

In addition to increasing  $Nu$ , corrugated channels also increase the loss of pressure and friction. The thermal–hydraulic performance factor (PEC) can be calculated for the revised model (nanofluid flow through the corrugated channel) using the reference model (water flow via the straight channel) as follows. In the design of thermal devices, PEC, as given in the equation, has become an important aspect to consider. For this reason, energy conservation requirements for such devices demand that heat transmission and friction losses be minimized. PR and ER ( $Nu$  enhancement ratio) were both critical to PEC performance. That is to say, the highest ER and the lowest PR outputs, respectively offer the best PEC.

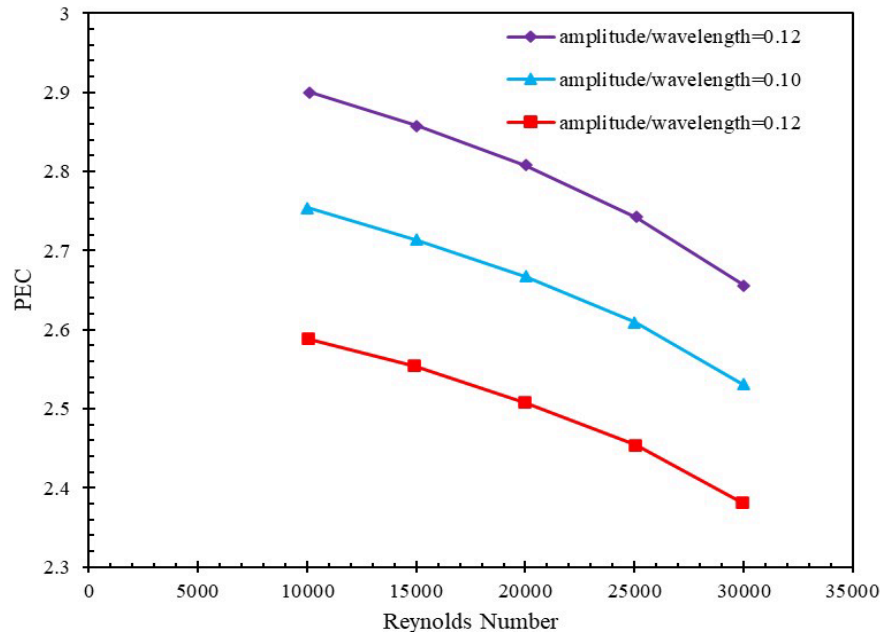


Figure 35: The effects of different values of the trapezoidal-corrugated channel's amplitude to wavelength ratio on PEC

PEC is also seen to decrease with time as Re is raised. For example, at Reynolds numbers between 10,000 and 30,000, amplitude/wavelength=0.08, 0.1, and 0.12, respectively, lead to 1.82 percent, 9.11 percent, 8.66 percent, and 9.22 percent reductions in PEC. This means that for a given heat load and pressure drop, trapezoidal-corrugated channels with high amplitude/wavelength ratios can provide the best PEC with the most heat transfer enhancement for the given pressure drop.

## CHAPTER 5

### CONCLUSION AND RECOMMENDATION

The results of our proposed heat transfer enhancement of the double dimpled corrugated pipe are summarized in this section. To prepare for a more comprehensive investigation with a wider reach in the near future, this section has been expanded to describe the study's shortcomings.

#### 5.1 Findings

Our study introduced the incorporation of both Nano fluid and hybrid nanofluid as the cooling medium in the heat exchanger. This serves as a state-of-the-art technology regarding the cooling solution for heat exchanger. Our study has tried to contribute to this field with a detailed performance comparison of different conventionally used base fluid and nanoparticle combinations. The findings of our study can be stated as following:

- The computational and experimental results are in good agreement. Nusselt number values increase with increasing Re numbers. A maximum fluctuation error of 5% exists between the two outcomes.
- Thermal hydraulic performance is significantly influenced by changes in the corrugation geometrical configurations. Flow separation, turbulence, boundary layer dispersion, and flow mixing all increase because of these changes. As a result, corrugated pipes offer a significant advantage over smooth pipes.
- As the aspect ratio of corrugated pipe is decreased, this will enhance the amount of heat being transferred. With the use of a corrugated pattern, the flow along its surface is regulated. As a result, the heat transfer coefficient over the corrugated surface is enhanced. The heat transfer coefficients ( $h$ ) for the pipes with aspect ratios of 2, 2.5, and 3 were 20%, 15%, and 12% greater than for the smooth pipe with a Re of 20000, respectively. Thus, simulated findings indicate that utilizing various AR improves thermal performance.
- The coefficient of friction,  $f$  is much greater for surfaces with corrugated geometries. The causes are mixing flow, the influence of corrugated surface regions and vortex flow of the fluid. It is actually the numerous geometrical

configurations of dimple corrugated surfaces that contribute to the friction induced by pressure drop throughout the pipe.

- Corrugated pipes can surpass smooth ones because the PEC value is higher than one. Increasing the geometric arrangement (number of dimple in corrugation) of the corrugated pipe results in a significant rise in both the pressure drop and the Nu. In geometries with corrugated surfaces, the Nu number enhancement increases in proportion to the Re number. The nanofluid with the largest PEC is 1% Al<sub>2</sub>O<sub>3</sub>/water at Re = 10000, which is 23% greater than the base fluid.
- Decreasing the aspect ratio of the inner pipe reduces its cross section, hence increasing the flow velocity. Furthermore, when the aspect ratio of the inner pipe lowers, the entry length increases, indicating a prolonged flow development. As the aspect ratio of the channel increases, greater buoyancy levels are required to enhance heat transfer.
- When dimple diameters increase, the average pipe temperature rises as compared to a smooth pipe. Because of these changes in temperature variances, it is possible to improve overall heat transfer performance.
- As the volume percentage of each nanofluid increases, the volumetric entropy generation decreases. Furthermore, the volumetric entropy generation at 1%, 2%, and 3% was highest for Al<sub>2</sub>O<sub>3</sub>/water, Al<sub>2</sub>O<sub>3</sub>-CuO/water, and CuO/water, respectively.
- Corrugated pipe has a greater total heat transfer efficiency than smooth pipe. As a result, by enhancing thermal performance, a more cost-effective heat exchanger can be designed.

## 5.2 Limitations

Despite having strong consistency and accuracy with reference experimental data, we have some restrictions and constraints because our entire study is based on numerical simulation. A larger volume proportion of nanoparticles may be added to the base fluid because of its high surface tension. We have tried to contribute to this subject by conducting a detailed comparison of the properties of several nanofluid combinations and the ideal cooling range for each one. The limitations of our numerical model are discussed below:

- There is no universal model for the determination of nanofluid mixture properties. Implementation of each model depends on the combination and context of the problem.
- Prediction of the flow field and heat transfer phenomena for high velocity flow and high source heat flux is very challenging and intangible.
- Nanoparticles with a large surface area to volume ratio have a high surface energy. The nanoparticles form agglomeration to reduce their surface energy. The attraction of van der Waals forces between nanoparticles causes them to agglomerate uncontrollably. Flow in the heat exchanger is greatly disturbed when agglomeration occurs, which has an adverse influence on the sink's overall performance. There is no way to regulate or forecast this phenomenon numerically.

### **5.3 Future Recommendation**

Several directions for further research are opened up because of this research, including experimental and simulation studies. The results of this work and others indicate that the use of nanofluids in turbulent flow will result in increased heat transfer. The heat transfer process in these systems may be better understood if the particle geometry is altered from the spherical 40 nm particles employed in this study. Particles of smaller sizes may lead to higher increases because of the increased surface area of the particle touching the fluid, according to earlier research. Different mixing and surface area augmentation effects may be introduced because of this. The thermal conductivity of the particles appears to be linked to the improvement of heat transfer. The use of higher thermal conductivity materials like Al and Cu, such as those in our study, could lead to even greater improvements. Before conducting these experiments, it is strongly recommended that a design of experiments be prepared to minimize the time needed to collect statistically meaningful data due to the huge number of experimental variables present in this system.

Nanofluids must be deployed in commercially relevant systems to show their potential performance advantages over currently used heat transfer fluids. The cooling of high-speed CPUs and microprocessors could be a potential use for this technology. Simulations can be used to help develop a heat transfer system that can take use of the



nanoparticles in the nanofluid. Additional simulations would be required to prove that the particles could break through the thermal boundary layer in the area of greatest heat exchange, i.e. flow through a slit with a heated side. In light of the simulation's findings, a working demonstration system might be constructed and put to the test.

## REFERENCES

- [1] A. S. Ahuja, “Augmentation of heat transport in laminar flow of polystyrene suspensions. I. Experiments and results,” *J. Appl. Phys.*, vol. 46, no. 8, pp. 3408–3416, Aug. 1975, doi: 10.1063/1.322107.
- [2] N. Nikkam, *Engineering Nanofluids for Heat Transfer Applications*. 2014.
- [3] W. Wang, Y. Zhang, B. Li, and Y. Li, “Numerical investigation of tube-side fully developed turbulent flow and heat transfer in outward corrugated tubes,” *Int. J. Heat Mass Transf.*, vol. 116, pp. 115–126, 2018, doi: <https://doi.org/10.1016/j.ijheatmasstransfer.2017.09.003>.
- [4] J. Alhamid and R. A. Al-Obaidi, “Flow pattern investigation and thermohydraulic performance enhancement in three-dimensional circular pipe under varying corrugation configurations,” in *Journal of Physics: Conference Series*, 2021, vol. 1845, no. 1, p. 12061.
- [5] W. Wang, Y. Zhang, K.-S. Lee, and B. Li, “Optimal design of a double pipe heat exchanger based on the outward helically corrugated tube,” *Int. J. Heat Mass Transf.*, vol. 135, pp. 706–716, 2019, doi: <https://doi.org/10.1016/j.ijheatmasstransfer.2019.01.115>.
- [6] A. R. Al-Obaidi and I. Chaer, “Study of the flow characteristics, pressure drop and augmentation of heat performance in a horizontal pipe with and without twisted tape inserts,” *Case Stud. Therm. Eng.*, vol. 25, p. 100964, 2021.
- [7] N. Kurtulmuş and B. Sahin, “Experimental investigation of pulsating flow structures and heat transfer characteristics in sinusoidal channels,” *Int. J. Mech. Sci.*, vol. 167, p. 105268, 2020, doi: <https://doi.org/10.1016/j.ijmecsci.2019.105268>.
- [8] W. Wang, Y. Shuai, B. Li, B. Li, and K.-S. Lee, “Enhanced heat transfer performance for multi-tube heat exchangers with various tube arrangements,” *Int. J. Heat Mass Transf.*, vol. 168, p. 120905, 2021, doi: <https://doi.org/10.1016/j.ijheatmasstransfer.2021.120905>.
- [9] A. R. Al-Obaidi, “Analysis of the Effect of Various Impeller Blade Angles on

- Characteristic of the Axial Pump with Pressure Fluctuations Based on Time- and Frequency-Domain Investigations,” *Iran. J. Sci. Technol. Trans. Mech. Eng.*, vol. 45, no. 2, pp. 441–459, 2021, doi: 10.1007/s40997-020-00392-3.
- [10] N. Kurtulmuş and B. Sahin, “A review of hydrodynamics and heat transfer through corrugated channels,” *Int. Commun. Heat Mass Transf.*, vol. 108, p. 104307, 2019, doi: <https://doi.org/10.1016/j.icheatmasstransfer.2019.104307>.
- [11] T. Alam and M.-H. Kim, “A comprehensive review on single phase heat transfer enhancement techniques in heat exchanger applications,” *Renew. Sustain. Energy Rev.*, vol. 81, pp. 813–839, 2018, doi: <https://doi.org/10.1016/j.rser.2017.08.060>.
- [12] T.-K. Hong, H.-S. Yang, and C. J. Choi, “Study of the enhanced thermal conductivity of Fe nanofluids,” *J. Appl. Phys.*, vol. 97, no. 6, p. 64311, 2005, doi: 10.1063/1.1861145.
- [13] H. J. Kim, I. C. Bang, and J. Onoe, “Characteristic stability of bare Au-water nanofluids fabricated by pulsed laser ablation in liquids,” *Opt. Lasers Eng.*, vol. 47, no. 5, pp. 532–538, 2009, doi: <https://doi.org/10.1016/j.optlaseng.2008.10.011>.
- [14] D. Ceotto and G. Croce, “Empirical equation for the prediction of viscosity for some common nanofluids,” *Colloid J.*, vol. 77, no. 2, pp. 244–247, 2015, doi: 10.1134/S1061933X15020040.
- [15] D. N. Chavda, J. Patel, H. Patel, and A. Parmar, “Effect of Nanofluid on Heat Transfer Characteristics of Double Pipe Heat Exchanger: Part : I : Effect of Aluminum Oxide Nanofluid,” *Int. J. Res. Eng. Technol. (IJRET)*, 2319-1163, vol. 3, pp. 42–52, 2014.
- [16] N. Gupta, S. Mishra, A. Tiwari, and S. Ghosh, “ScienceDirect A review of thermo physical properties of nanofluids,” *Mater. today Proc.*, vol. 18, 2019.
- [17] J. Albadr, S. Tayal, and M. Khazaal, “Heat transfer through heat exchanger using Al<sub>2</sub>O<sub>3</sub> nanofluid at different concentrations,” *Case Stud. Therm. Eng.*, vol. 1, pp. 38–44, 2013, doi: 10.1016/j.csite.2013.08.004.
- [18] B. Rahmati, A. A. D. Sarhan, and M. Sayuti, “Morphology of surface generated

by end milling AL6061-T6 using molybdenum disulfide (MoS<sub>2</sub>) nanolubrication in end milling machining,” *J. Clean. Prod.*, vol. 66, pp. 685–691, 2014.

- [19] Y. Vermahmoudi, S. M. Peyghambarzadeh, S. H. Hashemabadi, and M. Naraki, “Experimental investigation on heat transfer performance of Fe<sub>2</sub>O<sub>3</sub>/water nanofluid in an air-finned heat exchanger,” *Eur. J. Mech. - B/Fluids*, vol. 44, pp. 32–41, 2014, doi: <https://doi.org/10.1016/j.euromechflu.2013.10.002>.
- [20] C. L. Altan, B. Gurten, N. A. J. M. Sommerdijk, and S. Bucak, “Deterioration in effective thermal conductivity of aqueous magnetic nanofluids,” *J. Appl. Phys.*, vol. 116, no. 22, p. 224904, 2014, doi: 10.1063/1.4902441.
- [21] S. S. Raja, K. C. K. Vijayakumar, and R. Gangadevi, “Effects of Specific Fuel Consumption and Exhaust Emissions of Four Stroke Diesel Engine with CuO/Water Nanofluid as Coolant,” *Arch. Mech. Eng.*, vol. 64, 2017, doi: 10.1515/meceng-2017-0007.
- [22] A. A. Abbasian Arani and J. Amani, “Experimental investigation of diameter effect on heat transfer performance and pressure drop of TiO<sub>2</sub>–water nanofluid,” *Exp. Therm. Fluid Sci.*, vol. 44, pp. 520–533, 2013, doi: <https://doi.org/10.1016/j.expthermflusci.2012.08.014>.
- [23] K. Sharma, W. Azmi, S. Kamal, and S. Hassan, “Numerical Analysis of Experimental Turbulent Forced Convection Heat Transfer for Nanofluid Flow in a Tube,” *Appl. Mech. Mater.*, vol. 819, pp. 132–141, 2016, doi: 10.4028/www.scientific.net/AMM.819.132.
- [24] S. Sen Gupta *et al.*, “Thermal conductivity enhancement of nanofluids containing graphene nanosheets,” *J. Appl. Phys.*, vol. 110, no. 8, p. 84302, 2011, doi: 10.1063/1.3650456.
- [25] X. Xu, H. Li, and G. Xian, “Energy dissipation behaviors of surface treated multi-walled carbon nanotubes-based nanofluid,” *Mater. Lett.*, vol. 66, no. 1, pp. 176–178, 2012.
- [26] M. Kole and T. K. Dey, “Enhanced thermophysical properties of copper nanoparticles dispersed in gear oil,” *Appl. Therm. Eng.*, vol. 56, no. 1–2, pp. 45–53, 2013.

- [27] M. N. Rashin and J. Hemalatha, "Viscosity studies on novel copper oxide-coconut oil nanofluid," *Exp. Therm. Fluid Sci.*, vol. 48, pp. 67–72, 2013.
- [28] R. Khedkar, A. Kiran, S. Sonawane, K. Wasewar, and S. Umre, "Thermo – Physical Characterization of Paraffin based Fe<sub>3</sub>O<sub>4</sub> Nanofluids," *Procedia Eng.*, vol. 51, pp. 342–346, 2013, doi: 10.1016/j.proeng.2013.01.047.
- [29] F. Dökme and M. Turan, "Effects Of Using Pure Eco-Friendly Lubricants In Pump Bearings Instead Of Traditional Mineral Lubricants," 2016.
- [30] E. Ettefaghi, H. Ahmadi, A. Rashidi, A. Nouralishahi, and S. S. Mohtasebi, "Preparation and thermal properties of oil-based nanofluid from multi-walled carbon nanotubes and engine oil as nano-lubricant," *Int. Commun. Heat Mass Transf.*, vol. 46, no. Complete, pp. 142–147, 2013, doi: 10.1016/j.icheatmasstransfer.2013.05.003.
- [31] P. Keblinski, J. A. Eastman, and D. G. Cahill, "Nanofluids for thermal transport," *Mater. today*, vol. 8, no. 6, pp. 36–44, 2005.
- [32] L. Keemei, "STUDY OF FORCED CONVECTION NANOFLUID HEAT TRANSFER IN THE AUTOMOTIVE COOLING SYSTEM." 2016, doi: 10.13140/RG.2.1.3463.7202.
- [33] S. Senthilraja, M. Karthikeyan, and R. Gangadevi, "Nanofluid applications in future automobiles: comprehensive review of existing data," *Nano-Micro Lett.*, vol. 2, no. 4, pp. 306–310, 2010.
- [34] V. Vasu and K. M. Kumar, "Analysis of nanofluids as cutting fluid in grinding EN-31 steel," *Nano-Micro Lett.*, vol. 3, no. 4, pp. 209–214, 2011.
- [35] S. Khandekar, M. R. Sankar, V. Agnihotri, and J. Ramkumar, "Nano-Cutting Fluid for Enhancement of Metal Cutting Performance," *Mater. Manuf. Process.*, vol. 27, no. 9, pp. 963–967, 2012, doi: 10.1080/10426914.2011.610078.
- [36] M. Rahimi-Gorji, O. Pourmehran, M. Hatami, and D. D. Ganji, "Statistical optimization of microchannel heat sink (MCHS) geometry cooled by different nanofluids using RSM analysis," *Eur. Phys. J. Plus*, vol. 130, no. 2, pp. 1–21, 2015.

- [37] M. Karami, M. Bahabadi, S. Delfani, and A. Ghozatloo, "A new application of carbon nanotubes nanofluid as working fluid of low-temperature direct absorption solar collector," *Sol. Energy Mater. Sol. Cells*, vol. 121, pp. 114–118, 2014, doi: 10.1016/j.solmat.2013.11.004.
- [38] C. Yildiz, Y. Biçer, and D. Pehlivan, "Heat transfers and pressure drops in rotating helical pipes," *Appl. Energy*, vol. 50, no. 1, pp. 85–94, 1995, doi: [https://doi.org/10.1016/0306-2619\(95\)90765-9](https://doi.org/10.1016/0306-2619(95)90765-9).
- [39] P. G. Vicente, A. García, and A. Viedma, "Experimental investigation on heat transfer and frictional characteristics of spirally corrugated tubes in turbulent flow at different Prandtl numbers," *Int. J. Heat Mass Transf.*, vol. 47, no. 4, pp. 671–681, 2004, doi: <https://doi.org/10.1016/j.ijheatmasstransfer.2003.08.005>.
- [40] D. Yang, Y. Guo, and J. Zhang, "Evaluation of the thermal performance of an earth-to-air heat exchanger (EAHE) in a harmonic thermal environment," *Energy Convers. Manag.*, vol. 109, pp. 184–194, 2016, doi: <https://doi.org/10.1016/j.enconman.2015.11.050>.
- [41] T. Ma, L. Li, X.-Y. Xu, Y.-T. Chen, and Q.-W. Wang, "Study on local thermal–hydraulic performance and optimization of zigzag-type printed circuit heat exchanger at high temperature," *Energy Convers. Manag.*, vol. 104, pp. 55–66, 2015, doi: <https://doi.org/10.1016/j.enconman.2015.03.016>.
- [42] P. S. Kathait and A. K. Patil, "Thermo-hydraulic performance of a heat exchanger tube with discrete corrugations," *Appl. Therm. Eng.*, vol. 66, no. 1, pp. 162–170, 2014, doi: <https://doi.org/10.1016/j.applthermaleng.2014.01.069>.
- [43] Y. Dong, L. Huixiong, and C. Tingkuan, "Pressure drop, heat transfer and performance of single-phase turbulent flow in spirally corrugated tubes," *Exp. Therm. Fluid Sci.*, vol. 24, no. 3, pp. 131–138, 2001, doi: [https://doi.org/10.1016/S0894-1777\(01\)00047-4](https://doi.org/10.1016/S0894-1777(01)00047-4).
- [44] H. G. Kwon, S. D. Hwang, and H. H. Cho, "Flow and heat/mass transfer in a wavy duct with various corrugation angles in two dimensional flow regimes," *Heat mass Transf.*, vol. 45, no. 2, pp. 157–165, 2008.
- [45] V. D. Zimparov, N. L. Vulchanov, and L. B. Delov, "Heat transfer and friction

- characteristics of spirally corrugated tubes for power plant condensers—1. Experimental investigation and performance evaluation,” *Int. J. Heat Mass Transf.*, vol. 34, no. 9, pp. 2187–2197, 1991, doi: [https://doi.org/10.1016/0017-9310\(91\)90045-G](https://doi.org/10.1016/0017-9310(91)90045-G).
- [46] P. G. Vicente, A. García, and A. Viedma, “Heat transfer and pressure drop for low Reynolds turbulent flow in helically dimpled tubes,” *Int. J. Heat Mass Transf.*, vol. 45, no. 3, pp. 543–553, 2002, doi: [https://doi.org/10.1016/S0017-9310\(01\)00170-3](https://doi.org/10.1016/S0017-9310(01)00170-3).
- [47] C. Thianpong, P. Eiamsa-Ard, K. Wongcharee, and S. Eiamsa-Ard, “Compound heat transfer enhancement of a dimpled tube with a twisted tape swirl generator,” *Int. Commun. heat mass Transf.*, vol. 36, no. 7, pp. 698–704, 2009.
- [48] Y. Rao, C. Wan, and Y. Xu, “An experimental study of pressure loss and heat transfer in the pin fin-dimple channels with various dimple depths,” *Int. J. Heat Mass Transf.*, vol. 55, no. 23–24, pp. 6723–6733, 2012.
- [49] C. Bi, G. H. Tang, and W. Q. Tao, “Heat transfer enhancement in mini-channel heat sinks with dimples and cylindrical grooves,” *Appl. Therm. Eng.*, vol. 55, no. 1–2, pp. 121–132, 2013.
- [50] X. Lei, J. Shuang, P. Yang, and Y. Liu, “Parametric study and optimization of dimpled tubes based on Response Surface Methodology and desirability approach,” *Int. J. Heat Mass Transf.*, vol. 142, p. 118453, 2019.
- [51] Q. Fan and X. Yin, “3-D numerical study on the effect of geometrical parameters on thermal behavior of dimple jacket in thin-film evaporator,” *Appl. Therm. Eng.*, vol. 28, no. 14–15, pp. 1875–1881, 2008.
- [52] M. Esmaili, K. Sadeghy, and M. Moghaddami, “Heat transfer enhancement of wavy channels using Al<sub>2</sub>O<sub>3</sub> nanoparticles,” *J. Enhanc. Heat Transf.*, vol. 17, no. 2, 2010.
- [53] S. D. Pandey and V. K. Nema, “Experimental analysis of heat transfer and friction factor of nanofluid as a coolant in a corrugated plate heat exchanger,” *Exp. Therm. Fluid Sci.*, vol. 38, pp. 248–256, 2012.

- [54] M. Khoshvaght-Aliabadi, A. Zamzamian, and F. Hormozi, "Wavy channel and different nanofluids effects on performance of plate-fin heat exchangers," *J. Thermophys. Heat Transf.*, vol. 28, no. 3, pp. 474–484, 2014.
- [55] R. Gupta, P. E. Geyer, D. F. Fletcher, and B. S. Haynes, "Thermohydraulic performance of a periodic trapezoidal channel with a triangular cross-section," *Int. J. Heat Mass Transf.*, vol. 51, no. 11–12, pp. 2925–2929, 2008.
- [56] N. Tokgoz, T. Tunay, and B. Sahin, "Effect of corrugated channel phase shifts on flow structures and heat transfer rate," *Exp. Therm. Fluid Sci.*, vol. 99, pp. 374–391, 2018.
- [57] R. K. Ajeel, W.-I. Salim, and K. Hasnan, "Design characteristics of symmetrical semicircle-corrugated channel on heat transfer enhancement with nanofluid," *Int. J. Mech. Sci.*, vol. 151, pp. 236–250, 2019.
- [58] R. K. Ajeel, W. S.-I. W. Salim, and K. Hasnan, "Heat transfer enhancement in semicircle corrugated channel: effect of geometrical parameters and nanofluid," *J. Adv. Res. Fluid Mech. Therm. Sci.*, vol. 53, no. 1, pp. 82–94, 2019.
- [59] R. K. Ajeel *et al.*, "Turbulent convective heat transfer of silica oxide nanofluid through corrugated channels: An experimental and numerical study," *Int. J. Heat Mass Transf.*, vol. 145, p. 118806, 2019.
- [60] K. Narrein and H. A. Mohammed, "Influence of nanofluids and rotation on helically coiled tube heat exchanger performance," *Thermochim. Acta*, vol. 564, pp. 13–23, 2013.
- [61] M. A. Khairul, R. Saidur, M. M. Rahman, M. A. Alim, A. Hossain, and Z. Abidin, "Heat transfer and thermodynamic analyses of a helically coiled heat exchanger using different types of nanofluids," *Int. J. Heat Mass Transf.*, vol. 67, pp. 398–403, 2013.
- [62] T. Srinivas and A. V. Vinod, "Heat transfer intensification in a shell and helical coil heat exchanger using water-based nanofluids," *Chem. Eng. Process. Process Intensif.*, vol. 102, pp. 1–8, 2016.
- [63] N. Kannadasan, R. Kalimuthu, and S. Sivan, "Comparison of heat transfer and pressure drop in horizontal and vertical helically coiled heat exchanger with



- CuO/water based nano fluids,” *Exp. Therm. Fluid Sci.*, vol. 42, pp. 64–70, 2012, doi: 10.1016/j.expthermflusci.2012.03.031.
- [64] M. Shafahi, V. Bianco, K. Vafai, and O. Manca, “An investigation of the thermal performance of cylindrical heat pipes using nanofluids,” *Int. J. Heat Mass Transf.*, vol. 53, no. 1–3, pp. 376–383, 2010.
- [65] Z. Wu, L. Wang, and B. Sundén, “Pressure drop and convective heat transfer of water and nanofluids in a double-pipe helical heat exchanger,” *Appl. Therm. Eng.*, vol. 60, no. 1–2, pp. 266–274, 2013.
- [66] S. Suresh, K. P. Venkataraj, P. Selvakumar, and M. Chandrasekar, “Synthesis of Al<sub>2</sub>O<sub>3</sub>--Cu/water hybrid nanofluids using two step method and its thermo physical properties,” *Colloids Surfaces A Physicochem. Eng. Asp.*, vol. 388, no. 1–3, pp. 41–48, 2011.
- [67] Z. Aparna, M. Michael, S. K. Pabi, and S. Ghosh, “Thermal conductivity of aqueous Al<sub>2</sub>O<sub>3</sub>/Ag hybrid nanofluid at different temperatures and volume concentrations: an experimental investigation and development of new correlation function,” *Powder Technol.*, vol. 343, pp. 714–722, 2019.
- [68] L. S. Sundar, M. K. Singh, and A. C. M. Sousa, “Enhanced heat transfer and friction factor of MWCNT--Fe<sub>3</sub>O<sub>4</sub>/water hybrid nanofluids,” *Int. Commun. Heat Mass Transf.*, vol. 52, pp. 73–83, 2014.
- [69] D. Huang, Z. Wu, and B. Sunden, “Effects of hybrid nanofluid mixture in plate heat exchangers,” *Exp. Therm. Fluid Sci.*, vol. 72, pp. 190–196, 2016.
- [70] V. Kumar, A. K. Tiwari, and S. K. Ghosh, “Effect of variable spacing on performance of plate heat exchanger using nanofluids,” *Energy*, vol. 114, pp. 1107–1119, 2016.
- [71] A. Bhattad, J. Sarkar, and P. Ghosh, “Discrete phase numerical model and experimental study of hybrid nanofluid heat transfer and pressure drop in plate heat exchanger,” *Int. Commun. Heat Mass Transf.*, vol. 91, pp. 262–273, 2018.
- [72] A. Bhattad, J. Sarkar, and P. Ghosh, “Exergetic analysis of plate evaporator using hybrid nanofluids as secondary refrigerant for low-temperature applications,” *Int. J. Exergy*, vol. 24, no. 1, pp. 1–20, 2017.

- [73] A. Bhattad, J. Sarkar, and P. Ghosh, “Energy-economic analysis of plate evaporator using brine-based hybrid nanofluids as secondary refrigerant,” *Int. J. Air-Conditioning Refrig.*, vol. 26, no. 01, p. 1850003, 2018.
- [74] L. Xiao-wei, M. Ji-an, and L. Zhi-xin, “International Journal of Heat and Mass Transfer Roughness enhanced mechanism for turbulent convective heat transfer,” *Int. J. Heat Mass Transf.*, vol. 54, no. 9–10, pp. 1775–1781, 2011, doi: 10.1016/j.ijheatmasstransfer.2010.12.039.
- [75] M. Tekir, R. Ekiciler, and K. Arslan, “Numerical Simulation of Hybrid Nanofluid Flow in a Square Cross- Sectioned Horizontal Duct,” pp. 1–9.
- [76] I. F. D. D. B. T. L. AS, *Fundamentals of heat and mass transfer*. 2007.
- [77] H. H. A. D. Zi, *Development and Application of a Finite Volume Method for the Computation of Flows Around Moving Bodies on Unstructured , Overlapping Grids*, vol. M. 2005.
- [78] G. Araya, “Turbulence Model Assessment in Compressible Flows around Complex Geometries with Unstructured Grids,” 2019, doi: 10.3390/fluids4020081.
- [79] B. Takabi and H. Shokouhmand, “Effects of Al<sub>2</sub>O<sub>3</sub> – Cu/water hybrid nanofluid on heat transfer and flow characteristics in turbulent regime,” vol. 26, no. 4, pp. 1–25, 2015, doi: 10.1142/S0129183115500473.
- [80] Y. Khetib, H. M. Abo-dief, A. K. Alanazi, Z. Said, and S. Memon, “applied sciences The Influence of Forced Convective Heat Transfer on Hybrid Nanofluid Flow in a Heat Exchanger with Elliptical Corrugated Tubes : Numerical Analyses and Optimization,” 2022.
- [81] M. Ahsan, “ScienceDirect Numerical analysis of friction factor for a fully developed turbulent flow using  $k-\epsilon$  turbulence model with enhanced wall treatment,” vol. 3, pp. 2–10, 2014.
- [82] A. R. Al-obaidi, J. Alhamid, and H. Ali, “Effect of different corrugation interruptions Parameters on thermohydrodynamic characteristics and heat transfer performance of 3D Three-dimensional corrugated tube Case Studies in Thermal Engineering Effect of different corrugation interruptions Paramete,”

*Case Stud. Therm. Eng.*, vol. 32, no. March, p. 101879, 2022, doi: 10.1016/j.csite.2022.101879.

- [83] M. Omid and M. Farhadi, “Numerical study on the effect of using spiral tube with lobed cross section in double-pipe heat exchangers,” *J. Therm. Anal. Calorim.*, vol. 134, no. 3, pp. 2397–2408, 2018, doi: 10.1007/s10973-018-7579-y.
- [84] F. Pourfattah, M. Motamedian, G. Sheikhzadeh, and D. Toghraie, “International Journal of Mechanical Sciences The numerical investigation of angle of attack of inclined rectangular rib on the turbulent heat transfer of Water-Al<sub>2</sub>O<sub>3</sub> nanofluid in a tube,” *Int. J. Mech. Sci.*, vol. 131–132, no. August, pp. 1106–1116, 2017, doi: 10.1016/j.ijmecsci.2017.07.049.
- [85] *Fluent 6.3 user guide*, no. September. Fluent Inc., Lebanon, 2006.
- [86] I. B. Celik and J. Li, “Assessment of numerical uncertainty for the calculations of turbulent flow over a backward-facing step,” no. August, pp. 1015–1031, 2005.
- [87] J. A. Eastman, “THERMAL TRANSPORT IN NANOFUIDS1,” 2004, doi: 10.1146/annurev.matsci.34.052803.090621.
- [88] J. Sarkar, “A critical review on convective heat transfer correlations of nanofluids,” *Renew. Sustain. Energy Rev.*, vol. 15, no. 6, pp. 3271–3277, 2011, doi: 10.1016/j.rser.2011.04.025.
- [89] C. Series, “Investigation of convective heat transfer enhancement for nanofluid flow over flat plate Investigation of convective heat transfer enhancement for nanofluid flow over flat plate,” 2020, doi: 10.1088/1742-6596/1564/1/012007.
- [90] M. Massoudi and T. X. Phuoc, “Remarks on Constitutive Modeling of Nanofluids,” vol. 2012, 2012, doi: 10.1155/2012/927580.
- [91] A. Bibi and H. Xu, “Free convection of a hybrid nanofluid past a vertical plate embedded in a porous medium with anisotropic permeability,” no. December, 2019, doi: 10.1108/HFF-10-2019-0799.
- [92] T. Publications and F. U. Berlin, “Metastable, Mechanically Alloyed and Nanocrystalline Materials 1998,” vol. 314, pp. 629–634, 1999, doi:

10.4028/www.scientific.net/MSF.312-314.629.

- [93] U. Rea, T. Mckrell, L. Hu, and J. Buongiorno, “International Journal of Heat and Mass Transfer Laminar convective heat transfer and viscous pressure loss of alumina – water and zirconia – water nanofluids,” *Int. J. Heat Mass Transf.*, vol. 52, no. 7–8, pp. 2042–2048, 2009, doi: 10.1016/j.ijheatmasstransfer.2008.10.025.
- [94] Y. Xuan and W. Roetzel, “Conceptions for heat transfer correlation of nano fluids,” vol. 43, pp. 3701–3707, 2000.
- [95] H. C. Brinkman, “The Viscosity of Concentrated Suspensions and Solutions,” vol. 571, pp. 1–2, 1952, doi: 10.1063/1.1700493.
- [96] T. Hayat and S. Nadeem, “84G GE4AF98E 8A ; 4A68 @ 8AG J <G ; : H &,” *Results Phys.*, 2017, doi: 10.1016/j.rinp.2017.06.034.
- [97] A. Cyanamid, “TWO-COM PONENT SYSTEMS,” vol. 1, no. 3, pp. 187–191, 1959, doi: 10.1021/i160003a005.
- [98] S. Das, R. N. Jana, and O. D. Makinde, “Engineering Science and Technology , an International Journal Mixed convective magnetohydrodynamic fl ow in a vertical channel fi lled with nano fl uids,” pp. 1–12, 2015, doi: 10.1016/j.jestch.2014.12.009.
- [99] M. Gholinia, S. Gholinia, K. Hosseinzadeh, and D. D. Ganji, “Results in Physics Investigation on ethylene glycol Nano fl uid fl ow over a vertical permeable circular cylinder under e ff ect of magnetic fi eld,” vol. 9, no. March, pp. 1525–1533, 2018, doi: 10.1016/j.rinp.2018.04.070.
- [100] R. S. Vajjha and D. K. Das, “Development of new correlations for convective heat transfer and friction factor in turbulent regime for nanofluids,” no. April 2018, 2010, doi: 10.1016/j.ijheatmasstransfer.2010.06.032.
- [101] S. Dinarvand, M. N. Rostami, and I. Pop, “OPEN A novel hybridity model for TiO<sub>2</sub> - CuO / water hybrid nanofluid flow over a static / moving wedge or corner,” *Sci. Rep.*, pp. 1–11, 2019, doi: 10.1038/s41598-019-52720-6.
- [102] M. Reza, M. Goodarzi, and H. Alipour, “Investigation of rib ’ s height effect on heat transfer and flow parameters of laminar water – Al<sub>2</sub>O<sub>3</sub> nanofluid in a

- rib-microchannel,” *Appl. Math. Comput.*, vol. 290, pp. 135–153, 2016, doi: 10.1016/j.amc.2016.05.053.
- [103] E. Ebrahimnia-bajestan and F. Yazdanifard, “Performance of nanofluid-based photovoltaic / thermal systems : A review Performance of Nanofluid-Based Photovoltaic / Thermal Systems : A review,” no. July, 2017, doi: 10.1016/j.rser.2017.03.025.
- [104] R. Boushehri, H. Hassanzadeh, and A. Mousa, “Numerical investigation of magnetic field effect on nanofluid heat transfer in microchannel with hydrophobic surface using incompressible pre conditioned lattice Boltzmann method,” *SN Appl. Sci.*, vol. 2, no. 7, pp. 1–11, 2020, doi: 10.1007/s42452-020-2950-6.
- [105] I. Jiat, K. Wong, N. Tze, and A. Tiong, “Simulation approach on turbulent thermal performance factor of - Al<sub>2</sub>O<sub>3</sub> - Cu / water hybrid nanofluid in circular and non - circular ducts,” *SN Appl. Sci.*, vol. 3, no. 3, pp. 1–15, 2021, doi: 10.1007/s42452-021-04317-w.
- [106] B. Takabi and H. Shokouhmand, “Effects of Al<sub>2</sub>O<sub>3</sub>-Cu / water hybrid nanofluid on heat transfer and flow characteristics in turbulent regime,” no. August, 2015, doi: 10.1142/S0129183115500473.
- [107] M. R. Safaei, M. Gooarzi, O. A. Akbari, and M. S. Shadloo, “Performance Evaluation of Nanofluids in an Inclined Ribbed Microchannel for Electronic Cooling Applications.”
- [108] J. P. Meyer *et al.*, “The Viscosity of Nanofluids : A Review of the Theoretical , Empirical , and Numerical Models The Viscosity of Nanofluids : A Review of the Theoretical , Empirical , and Numerical Models,” vol. 7632, no. June, 2016, doi: 10.1080/01457632.2015.1057447.
- [109] M. N. Labib, J. Nine, H. Afrianto, H. Chung, and H. Jeong, “International Journal of Thermal Sciences Numerical investigation on effect of base fl uids and hybrid nano fl uid in forced convective heat transfer,” vol. c, pp. 163–171, 2013.
- [110] A. M. avood Domairry Ganji, *Heat Transfer Enhancement Using Nanofluid*

*Flow in Microchannels*. 2016.

- [111] S. Majid and J. Mohammad, “Optimal selection of annulus radius ratio to enhance heat transfer with minimum entropy generation in developing laminar forced,” pp. 1850–1865, 2017.
- [112] K. Khanafer and K. Vafai, “Synthesis of Mathematical Models Representing Bioheat Transport,” pp. 1–28, 2009.
- [113] P. Taylor and S. G. Kandlikar, “High Flux Heat Removal with Microchannels — A Roadmap of Challenges and Opportunities High Flux Heat Removal with Microchannels — A Roadmap of,” no. September 2013, pp. 37–41, 2007, doi: 10.1080/01457630591003655.
- [114] R. Faridi and G. Mahmood, “Numerical study of the effects of geometric parameters and nanofluid properties on heat transfer and pressure drop in helical tubes,” *SN Appl. Sci.*, no. June, 2021, doi: 10.1007/s42452-021-04701-6.
- [115] H. Ting and S. Hou, “Numerical Study of Laminar Flow and Convective Heat Transfer Utilizing Nanofluids in Equilateral Triangular Ducts with Constant Heat Flux,” 2016, doi: 10.3390/ma9070576.
- [116] S. Z. Heris, E. Talaii, and S. H. Noie, “CuO / Water Nanofluid Heat Transfer Through Triangular Ducts,” vol. 9, no. 1, pp. 23–32, 2012.
- [117] W. Lin, R. Shi, and J. Lin, “Heat Transfer and Pressure Drop of Nanofluid with Rod-like Particles in Turbulent Flows through a Curved Pipe,” 2022.
- [118] S. Z. Heris, S. H. Noie, E. Talaii, and J. Sargolzaei, “Numerical investigation of Al<sub>2</sub>O<sub>3</sub> / water nanofluid laminar convective heat transfer through triangular ducts,” *Nanoscale Res. Lett.*, vol. 6, no. 1, p. 179, 2011, doi: 10.1186/1556-276X-6-179.
- [119] V. Bianco, O. Manca, and S. Nardini, “Entropy generation analysis of turbulent convection flow of Al<sub>2</sub>O<sub>3</sub> – water nanofluid in a circular tube subjected to constant wall heat flux,” *Energy Convers. Manag.*, vol. 77, pp. 306–314, 2014, doi: 10.1016/j.enconman.2013.09.049.
- [120] E. B. Ratts, “Entropy Generation Minimization of Fully Developed Internal

Flow With Constant Heat Flux,” vol. 126, no. August 2004, pp. 656–659, 2019, doi: 10.1115/1.1777585.

- [121] A. Bejan and A. Bejan, “Entropy generation minimization : The new thermodynamics of finitesize devices and finitetime processes Entropy generation minimization : The new thermodynamics of finite-size devices and finite-time processes,” vol. 1191, no. 1996, 2012, doi: 10.1063/1.362674.
- [122] “ANSYS FLUENT Theory Guide,” vol. 15317, no. November, pp. 724–746, 2011.
- [123] E. S., “Investigation of the Enhancement of Convective Heat Transfer for Wall-Bounded Flows Utilizing Nanofluids,” 2017.
- [124] Alashkar A., “Evaluation of an Integrated PTSC/Thermal Energy Storage System Using Nano-Fluid Particle,” 2016.